Available online at www.sciencedirect.com
SCIENCE DIRECT®
Polymer 44 (2003) 4993–5013
polymer
www.elsevier.com/locate/polymer

Modeling properties of nylon 6/clay nanocomposites using composite theories

T.D. Fornes, D.R. Paul*

Department of Chemical Engineering and Texas Materials Institute, The University of Texas at Austin, Austin, TX 78712-1065, USA

Received 1 April 2003; received in revised form 19 May 2003; accepted 21 May 2003

Abstract

The reinforcement of nylon 6 by layered aluminosilicates (LAS) and glass fibers was examined using the composite theories of Halpin–Tsai and Mori–Tanaka. Theoretical comparisons show that exfoliated LAS offer superior reinforcement to glass fibers owing to the filler's high modulus, high aspect ratio, and its ability to reinforce in two directions. The effect of incomplete exfoliation of simple stacks of LAS on nanocomposite modulus was also examined. Increasing the number of platelets per stack and the gallery spacing between platelets results in a dramatic decrease in reinforcing efficiency. The predictions were benchmarked against experimental data for nylon 6 nanocomposites based on organically modified montmorillonite and glass fibers. The quantitative determination of the morphology of the nanocomposites is non-trivial due to the large distribution of filler shapes and sizes present. Thus, a detailed experimental procedure for determining the aspect ratio of the nanocomposites is reported. The composite theories satisfactorily capture the stiffness behavior of both types of composites. Furthermore, experimental heat distortion temperatures and those predicted from modeling the dynamic mechanical properties of nanocomposites are in reasonable agreement.

Keywords: Composite modeling; Polymer nanocomposites; Heat distortion temperature

1. Introduction

Polymer-layered aluminosilicate nanocomposites are of interest because they offer exceptional reinforcement at very low filler concentrations, often a fraction what is typically required with conventional fillers. This point is illustrated in Fig. 1; the modulus of nylon 6 is increased much more rapidly by addition of aluminosilicate platelets than by glass fibers. Specifically, doubling the modulus requires approximately 6.5 wt% layered silicate; whereas, three times this amount of glass fibers is needed to achieve the same increase. This advantage has significant implications since lower filler levels translate into lighter components, which is a desirable feature in many applications, especially in transportation where fuel efficiency is important. In addition, smaller sacrifices in matrix properties, e.g. ductility, impact strength, and surface finish, are often experienced with such nanocomposites.

Layered aluminosilicates (LAS) are composed of extremely thin (~1 nm), sheet-like platelets that possess very large surface areas and high aspect ratios. In addition, these platelets have an exceptionally high modulus in tension relative to most polymers and even many other fillers. Such properties enable the platelets, when dispersed in a polymer matrix, to carry a significant component of the applied load. Because of the high surface area and the small interparticle distances, the platelets can, in principle, significantly alter the properties of the polymer matrix [1–3], e.g. polymer crystalline morphology, chain conformation and dynamics through so-called confinement effects, etc. Thus, many factors could potentially be responsible for the property changes offered by these nanofillers, and a better understanding of the relative contribution from each source is needed. A significant question is whether the observed properties of nanocomposites can be explained by convention composite theory, which assumes that each phase has the same properties as if the other phase were not there, or whether one has to account for effects the filler has on the matrix. In principle, attempts to model the nanocomposite via composite theory provide a route to answering this question and a way to independently evaluate

* Corresponding author. Tel.: +1-512-471-5392; fax: +1-512-471-0542.
E-mail address: drp@che.utexas.edu (D.R. Paul).

0032-3861/03/$ - see front matter © 2003 Elsevier Science Ltd. All rights reserved.
doi:10.1016/S0032-3861(03)00471-3

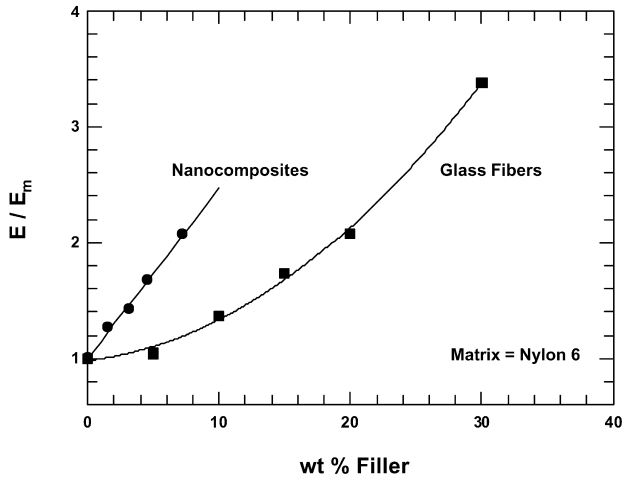

Fig. 1. Comparison of the reinforcement of nylon 6 by organically modified montmorillonite (nanocomposites) [23,24] and glass fibers [22]. Nanocomposite filler concentration is based on the wt% inorganic montmorillonite, since the aluminosilicate is the reinforcing component.

the individual effects of how matrix and filler modulus, filler geometry and orientation, etc. affect composite stiffness, at least within the assumption that one component does not affect the other. With this approach, one may be able to infer whether differences between observed and predicted behavior are due to changes in the polymer matrix induced by the filler or not. However, as will be shown here, there are many non-trivial issues involved in applying composite theories to nanocomposites.

The purpose of this paper is to better understand the origin of the superior reinforcing efficiency observed in well-exfoliated polymer–clay nanocomposites compared to conventional composites using composite theory. The theories of Halpin–Tsai and Mori–Tanaka are used to evaluate the effects of filler geometry, stiffness, and orientation. Model predictions are compared to experimental morphological and mechanical property data for both aluminosilicate nanocomposites and glass fiber composites based on nylon 6. The heat distortion temperatures (HDT) for nylon 6 nanocomposites, based on dynamic mechanical data, are compared to predictions by composite theory.

2. Background

Over several decades theoretical frameworks have been developed for predicting properties of composite materials based on the properties of the pure components and the morphology of the composite. An assumption inherent in all of these theories is that each component of the composite acts independently of the other. While the general objective of such theories is to predict performance of the composite for given set of components, these theories enable a simple route for evaluation of the individual contribution of component properties such as matrix and filler modulus, volume fraction, filler aspect ratio, filler orientation, etc. Aspect ratio is an important factor in polymer nanocomposites and drives an interest in achieving a high level of platelet exfoliation.

Halpin and Tsai developed a well known composite theory for predicting the stiffness of unidirectional composites as a function of aspect ratio [4–6]. This theory is based on the early micromechanics works of Hermans [7] and Hill [8]. Hermans generalized the form of Hill's self-consistent theory by considering a single fiber encased in a cylindrical shell of matrix, that is embedded an infinite medium assumed to possess the average properties of the composite. Halpin and Tsai reduced Hermans' results into a simpler analytical form adapted for a variety of reinforcement geometries, including discontinuous filler reinforcement. The longitudinal and transverse engineering moduli, E_{11} and E_{22}, are expressed in the general form

$$\frac{E}{E_m} = \frac{1 + \zeta\eta\phi_f}{1 - \eta\phi_f} \tag{1}$$

where E and E_m represent the Young's modulus of the composite and matrix, respectively, ζ is a shape parameter dependent upon filler geometry and loading direction, ϕ_f is the volume fraction of filler, and η is given by

$$\eta = \frac{E_f/E_m - 1}{E_f/E_m + \zeta} \tag{2}$$

where E_f represents the Young's modulus of the filler. By comparing model predictions with the two-dimensional finite element calculations of Foye [9] for discontinuous oriented square fiber-reinforced composites, Ashton et al. [6] determined that $\zeta = 2(a/b)$ provided good agreement for longitudinal modulus, E_{11}, where a and b are the length and thickness of the fiber. The modulus perpendicular to the fiber direction (transverse), on the other hand, was found to be relatively insensitive to fiber aspect ratio, and could be approximated by $\zeta = 2$ [6,10]. It should be noted that as $\zeta \rightarrow 0$ the Halpin–Tsai theory converges to the inverse rule of mixtures (lower bound), i.e.

$$\frac{1}{E} = \frac{\phi_f}{E_f} + \frac{(1 - \phi_f)}{E_m} \tag{3}$$

Conversely, when $\zeta \rightarrow \infty$ the theory reduces to the rule of mixtures (upper bound), i.e.

$$E = \phi_f E_f + (1 - \phi_f)E_m \tag{4}$$

Furthermore, the Halpin–Tsai equations retain the same form for discontinuous cylindrical fibers and lamellar shape reinforcements, such as ribbons or rectangular platelets; however, when calculating elastic moduli E_{11} and E_{22} in the case of ribbons or rectangular platelets, ζ is equal to (ℓ/t) and (w/t), respectively, where ℓ is the length, w is the width, and t is the thickness of the dispersed phase. Fig. 2(a) shows the two types of fillers examined in this work, their orientation with respect to orthogonal axes, and their corresponding Halpin–Tsai quantities; dispersed clay platelets are expected to resemble disks as depicted here;

(a)

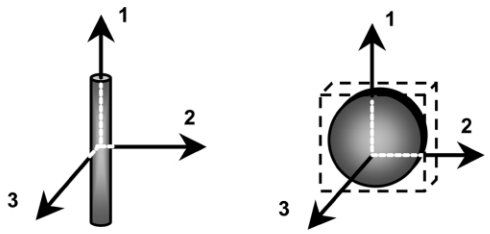

Fiber Disk-like Platelet

Direction of Applied Load	Halpin-Tsai Composite Modulus		Shape Parameter, $\zeta^{(a)}$	
	Fibers	Platelets	Fibers	Platelets
1	$E_{11} = E_{//}$	$E_{11} = E_{//}$	$\zeta = 2(l/d)$	$\zeta = 2(l/t)$
2	$E_{22} = E_{\perp}$	$E_{22} = E_{//}$	$\zeta = 2$	$\zeta = 2(l/t)$
3	$E_{33} = E_{\perp}$	$E_{33} = E_{\perp}$	$\zeta = 2$	$\zeta = 2$

(a) The symbol l represents the length of the fiber or diameter of the disk, d represents the fiber diameter, and t is thickness of the disk.

(b)

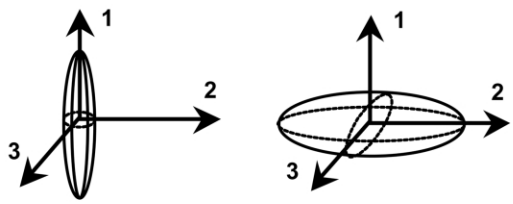

Fiber Disk-like Platelet

Direction of Applied Load	Mori-Tanaka Composite Modulus	
	Fibers	Platelets
1	$E_{11} = E_{//}$ (Eq. 5)	$E_{11} = E_{\perp}$ (Eq. 6)
2	$E_{22} = E_{\perp}$ (Eq. 6)	$E_{22} = E_{//}$ (Eq. 5)
3	$E_{33} = E_{\perp}$ (Eq. 6)	$E_{33} = E_{//}$ (Eq. 5)

Fig. 2. Physical representations, coordinate systems, and corresponding (a) Halpin–Tsai and (b) Mori–Tanaka equations used for the calculation of composite stiffness based on fiber and disk-like platelet reinforcement.

$E_{\|}$ and $E_{\perp}$ are the composite modulus parallel (longitudinal) and perpendicular (transverse) to the major axis of the filler.

The Mori–Tanaka average stress theory has also received considerable attention in the literature [11]. It was derived on the principles of Eshelby's inclusion model for predicting an elastic stress field in and around an ellipsoidal particle in an infinite matrix [12]. To account for finite filler concentrations, Mori and Tanaka [11], however, considered a non-dilute composite consisting of many identical spheroidal particles that cause the matrix to experience an average stress different from that of the applied stress; to satisfy equilibrium conditions the volume average over the entire composite was forced to equal the applied stress. Tandon and Weng [13] used this assumption and Eshelby's solution to derive complete analytical solutions for the elastic moduli of an isotropic matrix filled with aligned spheroidal inclusions. Their results for longitudinal and transverse elastic moduli are

$$\frac{E_{11}}{E_m} = \frac{A}{A + \phi_f(A_1 + 2\upsilon_m A_2)} \quad (5)$$

and

$$\frac{E_{22}}{E_m} = \frac{2A}{2A + \phi_f[-2\upsilon_0 A_3 + (1 - \upsilon_m)A_4 + (1 + \upsilon_m)A_5 A]} \quad (6)$$

where ϕ_f is the volume fraction of filler, ν_0 is the Poisson's ratio of the matrix, and A_1, A_2, A_3, A_4, A_5, and A are functions of the Eshelby's tensor and the properties of the filler and the matrix, specifically Young's modulus, Poisson's ratio, filler concentration and filler aspect ratio; complete details of these equations are given elsewhere [13]. It is important to note that the composite moduli in Eqs. (5) and (6) are dependent upon the shape of the filler, e.g. fiber-like versus disk-like ellipsoids, which are

accounted for in the Eshelby's tensor. Moreover, Eq. (6) is used instead of Eq. (5) when predicting modulus parallel to either major axis of a disk-like spheroid. Fig. 2(b) shows the Mori–Tanaka physical representation of glass fibers and disk-like platelets and tabularizes the different equations used to calculate composite moduli along the three principle orthogonal directions. Both the Halpin–Tsai equations and the Mori–Tanaka theory will be used in this work to evaluate polymer composites based on glass fibers and LAS.

A number of assumptions are inherent to both approaches; the filler and matrix are linearly elastic, isotropic, and firmly bonded. The filler is perfectly aligned, asymmetric, and uniform in shape and size. Particle–particle interactions are not explicitly considered. Of course, for all composite theories the properties of the matrix and filler are considered to be identical to those of the pure components. In addition to these assumptions, there are number of differences between the two theories that are worth noting. First, the Mori–Tanaka theory treats fibers and disks as ellipsoidal particles, whereas the Halpin–Tsai equations treat a fiber as a fiber and disk as a rectangular platelet; the later disparity in the Halpin–Tsai equations is of some concern, since the length and, in turn, aspect ratio across a disk is not constant as shown in Fig. 3. Second, the Halpin–Tsai equations for E_{11} and E_{22} are independent of the Poisson's ratio of the filler or the matrix. Third, the Halpin–Tsai equations for transverse modulus, i.e. perpendicular to the filler's major axis, are independent of aspect ratio (see Fig. 2(a)).

Last, it is important to emphasize that numerous complexities arise when comparing composite theory to experimental composite data, particularly for polymer layered silicate nanocomposites; Fig. 4 summarizes some of the issues involved. In addition to physical disparities between theory and experiment, the choice of composite theory will also dictate how well the predicted and observed properties agree. The Halpin–Tsai and Mori–Tanaka theories were chosen in this work based on their effectiveness in predicting stiffness of glass fiber reinforced composites, their adaptability for different filler geometries, particularly disks, and for their prevalence in the literature [5,13–24]; for a thorough review of micromechanical models for composite stiffness the reader is referred to the work of Tucker and Liang [22]. There are relatively few reports that deal specifically with nanocomposites [18–20,23,24].

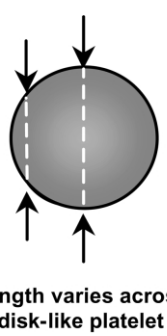

Fig. 3. Inherent variation in length, and subsequently aspect ratio, across a disk-like platelet.

Issue	Theory	Experimental
Filler shape and size	- Uniform shape - Constant dimensions	- Non-uniform shape - Distribution of lengths and thickness - Imperfect exfoliation of LAS
Filler orientation	- Unidirectional	- Some degree of misalignment
Filler interface	- The filler and matrix are well bonded	- Imperfect bonding between the filler and matrix
Filler modulus	- Assumes filler modulus is the same in all directions	- Filler is anisotropic
Matrix considerations	- Assumes matrix is isotropic	- Polymer chain orientation - Presence of polymer crystallites
Filler Concentration Effects	- No particle-particle interactions - Ignores changes in viscosity - No particle agglomeration	- Particle-particle interactions and agglomeration - Changes in viscosity can alter morphology during injection molding - Changes in crystalline morphology (e.g. type, crystallite size, and amount)

Fig. 4. Some important issues that limit the ability to model the stiffness properties of polymer–LAS nanocomposites.

3. Experimental

The following is a brief synopsis of the materials and procedures used to form the composites presented in this study. More complete details are given in prior publications from this laboratory [25–28].

3.1. Materials and composite preparation

Table 1 describes the materials used in this work [29]. Glass-fiber composites were formed into standard tensile bars (ASTM D638) by injection molding mixtures of a medium molecular weight, MMW, nylon 6 and pellets of a commercial product containing 30 wt% discontinuous glass fibers in nylon 6, BKV30, using an Arburg Allrounder 305-210-700 molding machine. Molding was conducted at a barrel temperature of 270 °C, mold temperature of 80 °C, injection pressure of 70 bar, and a holding pressure of 35 bar, respectively. Polymer nanocomposites were prepared by extruding mixtures of HMW nylon 6 pellets and organically modified montmorillonite, termed organoclay,

Table 1
Materials used in this study

Material [designation used here]	Supplier designation	Specifications	Supplier
Glass fiber/nylon 6 composites			
Nylon 6 [MMW]	Capron B73WP	$\bar{M}_n = 22,000$[a], MFI = 4.5 g/10 min	Honeywell (formerly AlliedSignal)
Glass fiber reinforced nylon 6 [BKV 30]	BKV 30	30 wt% well bonded, discontinuous, glass fibers, fiber diameter = 13 μm	Bayer
Organically modified montmorillonite/nylon 6 nanocomposites			
Nylon 6 [HMW]	Capron B135WP	$\bar{M}_n = 29,300$[a], MFI = 1.2 g/10 min	Honeywell (formerly AlliedSignal)
Organoclay [$(HE)_2M_1R_1$][b]	Bis(hydroxyethyl)-(methyl)-rapeseed quaternary ammonium organoclay	Organic loading = 95 mequiv./100 g clay, organic content = 34.1 wt%	Southern clay products

[a] $\bar{M}_n$, in units of Daltons, was determined via intrinsic viscosity using *m*-cresol at 25 °C [26].
[b] The substituents on the quaternary ammonium compound used to form the organoclay are identified in this shorthand notation where R = rapeseed, HE = hydroxyethyl, M = methyl. Rapeseed is natural product composed predominantly unsaturated C_{22} alkyl chains (45%).

using a Haake co-rotating twin screw extruder. The organoclay, designated here as $(HE)_2M_1R_1$, [26–28,30] was formed by a cation exchange reaction between sodium montmorillonite (CEC = 92 mequiv./100 g clay) and bis(hydroxyethyl)-(methyl)-rapeseed quaternary ammonium chloride. The amount of montmorillonite (MMT) present in the extruded composite was verified by placing pre-dried nanocomposite pellets in a furnace at 900 °C for 45 min. The resulting ash was weighed and corrected for loss of structural water [26,27]. Nanocomposite pellets were injection molded into tensile specimens under the same conditions listed above except using a slightly lower barrel temperature, 260 °C. In addition to producing tensile bars, Gardner disks having a diameter and thickness of 62 and 1.1 mm were fabricated for dynamic mechanical thermal analysis (DMTA). After molding, all specimens were immediately sealed in a polyethylene bag and placed in a vacuum desiccator for a minimum of 24 h prior to mechanical testing. It should be noted that all polyamide containing materials listed here were dried at 80 °C for at minimum of 16 h prior any melt processing step.

3.2. Mechanical properties

Tensile tests were conducted on both types of composites according to ASTM D638 using an Instron Model 1137 testing frame equipped with a computerized data acquisition system. Young's modulus was determined parallel to the polymer flow direction (FD), as indicated in Fig. 5(a), using an extensometer at a crosshead speed of 0.51 cm/min. Table 2 lists the modulus results obtained from the experiments.

In addition, the thermal-mechanical behavior of the nanocomposites was examined using a Mark III Rheometrics Scientific dynamic mechanical analyzer (DMTA). Experiments were carried out on test specimens approximately 25 mm in length, 10 mm in width, and 1.1 mm in thickness that were cut from injection molded Gardner disks as illustrated in Fig. 5(b). Specimens were simultaneously heated from −60 to 200 °C at a rate of 2 °C/min and analyzed for storage modulus (E'), loss modulus (E''), and tan δ, at a frequency of 1 Hz. The HDT for these materials was estimated from plots of log E' versus temperature using a technique developed by Scobbo [31]; the HDT is defined by ASTM standards (ASTM E2092) as the temperature at which the center deflection of a standard specimen in a three point bend mode reaches 0.25 mm under an applied maximum stress of either 0.46 or 1.82 MPa. The latter stress is typically employed for semi-crystalline and filled polymers. The HDT at a stress of 1.82 MPa corresponds to the temperature at which the logarithm of storage modulus (in Pa), log E', is 8.9.

3.3. Morphology characterization and determination of filler aspect ratio

The dispersion and orientation of glass fibers within the

Table 2
Young's modulus data for glass fiber composites and aluminosilicate nanocomposites based on nylon 6

wt% Glass fiber	vol% Glass fiber	Young's modulus (GPa)
Glass fiber—MMW nylon 6 composites		
0	0	2.84
5	2.3	2.96
10	4.75	3.88
15	7.34	4.93
20	10.1	5.89
30	16.1	9.60
wt% Inorganic (MMT)	vol% Inorganic (MMT)	Young's modulus (GPa)
$(HE)_2M_1R_1$—HMW nylon 6 composites		
0	0	2.75
1.6	0.65	3.49
3.2	1.31	3.92
4.6	1.91	4.59
7.2	3.03	5.70

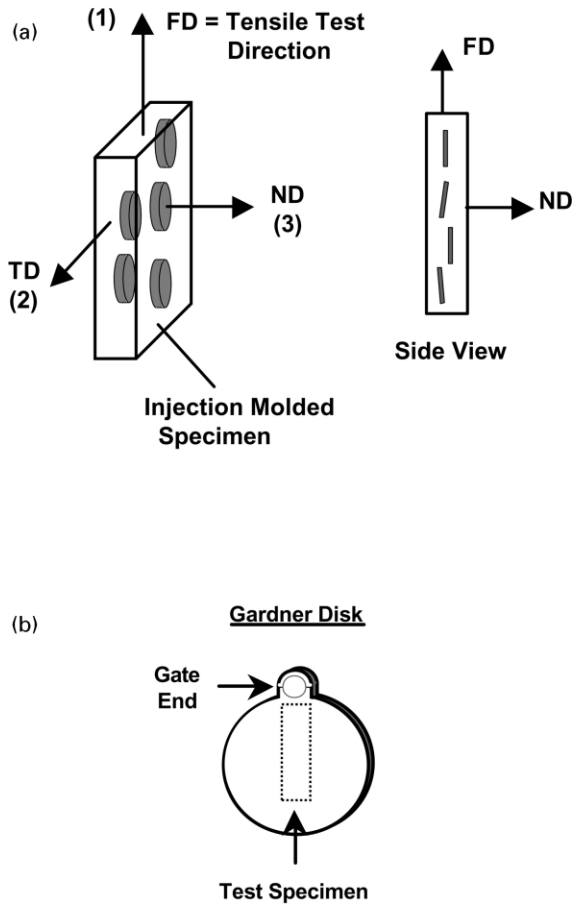

Fig. 5. Details of injection molded specimens used for (a) stress–strain and (b) DMTA analysis. Dispersed LAS are strongly oriented along the FD (tensile test direction) as previously demonstrated [23–25].

molded composites was examined using a JEOL JSM35C scanning electron microscope (SEM) as previously reported by Laura et al. [25]. In general, the outer portion or skin of the injection molded specimens exhibited a high degree of fiber alignment along the polymer FD; whereas, the central portion of the specimen exhibited a more random fiber orientation. Fiber lengths were measured via optical microscopy on fibers extracted from injection molded specimens. The extracted fibers (diameter = 13 μm) were obtained by first burning the polymer matrix in a furnace at 500 °C, then dispersing them in a 10 wt% solution of PMMA in toluene on glass slide, followed by solvent evaporation [25]. The average fiber length measured was 0.262 mm, which gives an aspect ratio (ℓ/d) of 20.

The morphology of injection molded nanocomposites was analyzed in detail using JOEL 2010 and 2010F transmission electron microscopes (TEM) as previously outlined [26–28]. It was found in these studies that high molecular grades of nylon 6, such as HMW, lead to exceptional exfoliation of $(HE)_2M_1R_1$ organoclay during melt processing. In addition, detailed morphological analyses of the interior of injection molded specimens showed that the dispersed platelets exhibit a high degree of orientation along the FD, as depicted in Fig. 5(a). TEM photomicrographs were also taken on sections extracted from the skin region of the specimens using a Phillips 208 TEM operating at an accelerating voltage of 100 kV. An even higher degree of orientation is observed (shown below) as compared to core photomicrographs. The exceptional exfoliation and good alignment of the platelets within these nanocomposites provided an excellent experimental candidate for comparison with composite theory. However, in order to model these composites, the aspect ratio of these composites must be determined.

Unlike glass fiber composites, the determination of filler aspect ratio for layered aluminosilicate nanocomposites is not straightforward. Good estimates require a thorough analysis of TEM photomicrographs at different magnifications. Fig. 6 depicts various complications of calculating an aspect ratio from TEM photomicrographs that arise from variations in both length, or diameter, and thickness. Clay platelets intrinsically have a distribution of lateral dimensions. The recovery, refinement, chemical treatment, and post-treatment of these clays may contribute to the variation in filler geometry. Furthermore, extrusion of these clays with polymer and any additional melt processing steps that follow, i.e. injection molding, will amplify the range of particle shapes and sizes, particularly when the LAS is not completely exfoliated as illustrated in Fig. 6. Finally, microtoming of the nanocomposite sample into thin sections for TEM analysis will also result in an apparent distribution of observed particle sizes even if all disk-like platelets were the same size. The experimental average length will thus be smaller than the true diameter; this effect is most severe when the thickness of the section is much less the platelet diameter. As section thickness increases to levels well beyond the particle diameter, however, the experimental average becomes much closer to the real value [29]. It is important to note the average section thickness here is on the order of 50 nm as compared to an average particle lateral dimension of 91 nm. In order to reduce the difficulties associated with aspect ratio estimation, a semi-automated procedure was employed to analyze TEM photomicrographs of the nanocomposites.

Accurate and reliable automated image analysis requires an original image having exceptional resolution and contrast; an ideal image would exhibit sharp transitions from black to white. In reality, a large majority of bright field TEM images of polymers consist of different shades of gray, which is primarily an indication of mass-thickness contrast throughout the sample. In the case of nanocomposites, contrast also arises from differences in atomic number within the materials, i.e. regions of high atomic number appear dark, while regions of low atomic number appear light. To the naked eye, discrimination between grayish polymeric regions and the dark lines corresponding to aluminosilicate platelets is relatively easy; however, this is not the case for most image analysis tools. Thus, analysis of polymer nanocomposites images necessitates conversion of

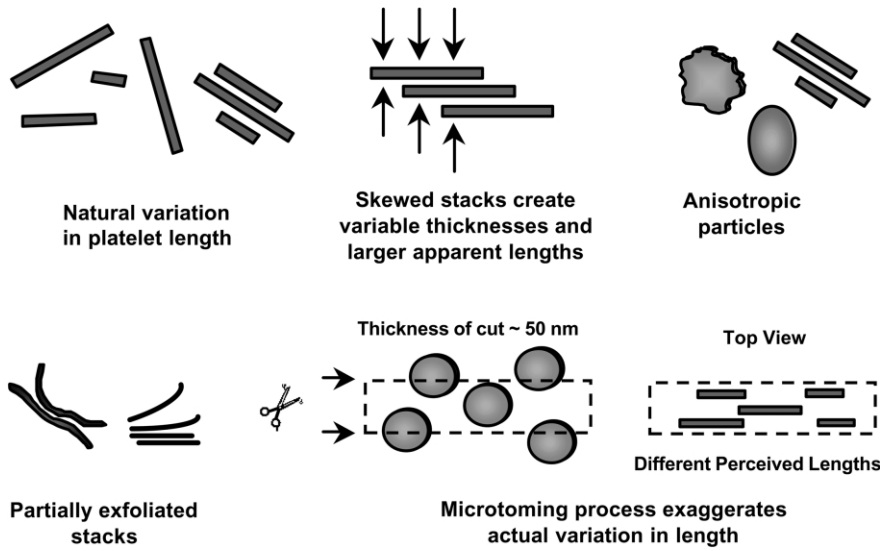

Fig. 6. Examples of complications in the determination of the aspect ratio of LAS fillers within polymer nanocomposites.

the original TEM photomicrograph into a black and white image using a semi-automated approach, as detailed below.

TEM images, typically in the range of 60 to 80 K in magnification for standard negative film, are first printed on 20.3×25.4 cm^2 photographic paper. Transparency film is placed over the print and dispersed platelets and/or agglomerates are traced over using a black permanent pen; agglomerates, immiscible, intercalated structures, and isolated platelets are treated as single particles. The resulting transparency is electronically scanned and converted into a grayscale tagged-image file format (TIFF) image file. This file is imported into the image analysis program (Scion Image 1.63 MacOS, National Institutes of Health). The program converts the TIFF image into a black and white image, creates a duplicate of the image, assigns each particle a numerical label, and exports the particle's length to a separate file. Fig. 7(a) shows a typical TEM photomicrograph of a nanocomposite and its corresponding processed TIFF image; in general, a much larger area is scanned than shown in Fig. 7(a). However, to have visible features after shrinking for journal publication, a portion of the 20.3×25.4 cm^2 TEM printout was used for Fig. 7(a). Fig. 8(a) shows a histogram of all MMT particle lengths and pertinent statistical data obtained on nanocomposite photomicrographs of sections taken from the core region of injection mold specimens parallel to the transverse direction (TD); since mechanical testing was conducted along FD, TEM sections for particle diameter characterization were cut from the FD–ND plane and viewed parallel to TD, as illustrated in the side view in Fig. 5(a). It is important to note that the length measurements were conducted at a constant filler concentration of 3.2 wt% MMT. The length may vary to some degree with filler concentration, however, previous TEM studies indicate the variation is small [26,27].

From a microscopy standpoint it is much easier to count the number of platelets within a small stack than it is to measure the stack thickness, especially since a wide variety of complex particle shapes are encountered as illustrated in Fig. 6. To count the number of platelets per particle, transparency film is placed over TEM high resolution photomicrographs, typically $\geq$80 K magnification, the number of platelets per particle is counted, and the resulting number is labeled on top of the particle. Last, the numbers are tabulated and statistically analyzed. Fig. 7(b) shows an example of a nanocomposite photomicrograph analyzed using this platelet counting technique. The statistical data for all particles analyzed using this platelet count technique is shown Fig. 8(b); it should be emphasized that these numbers are estimates and were obtained previously in a study of HMW nylon 6-$(HE)_2M_1R_1$ nanocomposites having low MMT contents, i.e. less than ~3 wt% [26,27].

The data presented in Fig. 7 are used to estimate the aspect ratio of the MMT particles as defined by

$$(\text{Aspect Ratio})_{\text{MMT}} = \frac{\bar{\ell}}{\bar{t}} \tag{7}$$

where $\bar{\ell}$ is the average particle length along the TD and $\bar{t}$ is the average particle thickness. For the distribution shown, the number average value is 91 nm ($\bar{\ell}_n$) while the weight average value is 118 nm ($\bar{\ell}_w$). For a perfectly exfoliated system, the average thickness of each particle is simply the thickness of a MMT platelet; this thickness may be calculated by adding the center-to-center distance between the outer oxygen atoms in the outer tetrahedral layers of sodium MMT [32,33] to twice the sum of the atomic radius oxygen, as shown in Fig. 9(a). The resulting value of 0.94 nm is in agreement with the interlayer spacings of pyrophillite (0.92 nm) and talc (0.94 nm) [34], which are the neutral forms of sodium montmorillonite; pyrophillite contains strictly aluminum, Al, atoms within the octahedral

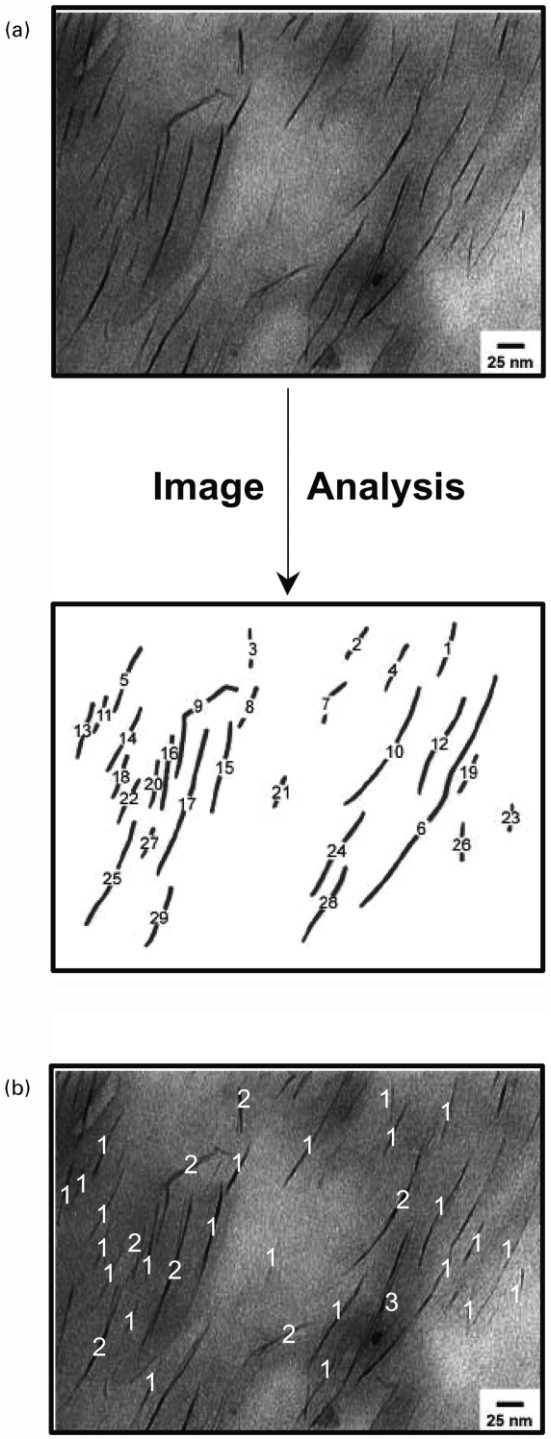

Fig. 7. Example of semi-automated analysis TEM images for determining (a) dispersed particle lengths and (b) the number of platelets per particle.

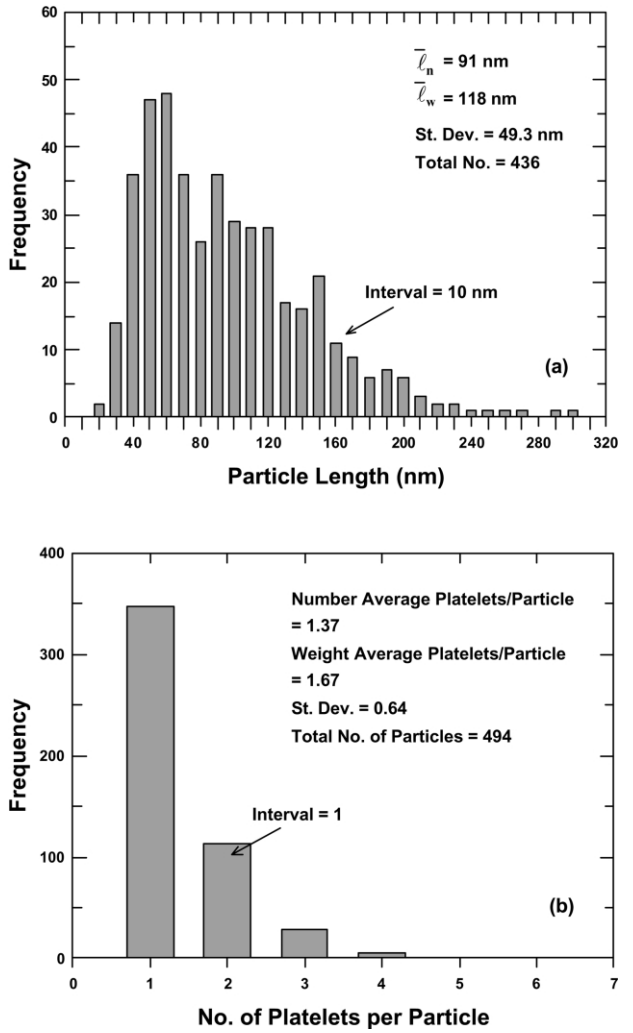

Fig. 8. Histogram of MMT (a) particle length [25] and (b) number of platelets per particle [23,24] for HMW nylon 6-$(HE)_2M_1R_1$ nanocomposites.

layer, while talc contains strictly magnesium, Mg. Sodium MMT of course contains a mixture of the two atoms, which is responsible for giving MMT its negative intralayer charge.

As mentioned earlier, direct calculation of thickness of an incompletely exfoliated particle is not trivial. Stacks of platelets may consist of residual unexchanged montmorillonite, non-expandable forms of clay, e.g. talc-like structures, collapsed organoclay in which the organic surfactant has been completely degraded or has escaped, etc. If the dispersed structure were pure montmorillonite or non-expandable clay, as depicted in Fig. 9(b), the thickness of each particle may be calculated by

$$t^{(u)}_{particle} = d^{(u)}_{001}(n-1) + t_{platelet} \quad (8)$$

where $d^{(u)}_{001}$ is the repeat spacing of sodium MMT, i.e. 0.96 nm, n is the number of platelets per particle, and $t_{platelet}$ is the thickness of a MMT platelet, estimated above to be 0.94 nm. Experimentally, though, it is believed that a majority of platelet stacks in the present nanocomposites are organoclay stacks that have been intercalated by polymer to various degrees, as depicted in Fig. 9(c). In this scheme, particle thickness is defined as

$$t^{(i)}_{particle} = d^{(i)}_{001}(n-1) + t_{platelet} \quad (9)$$

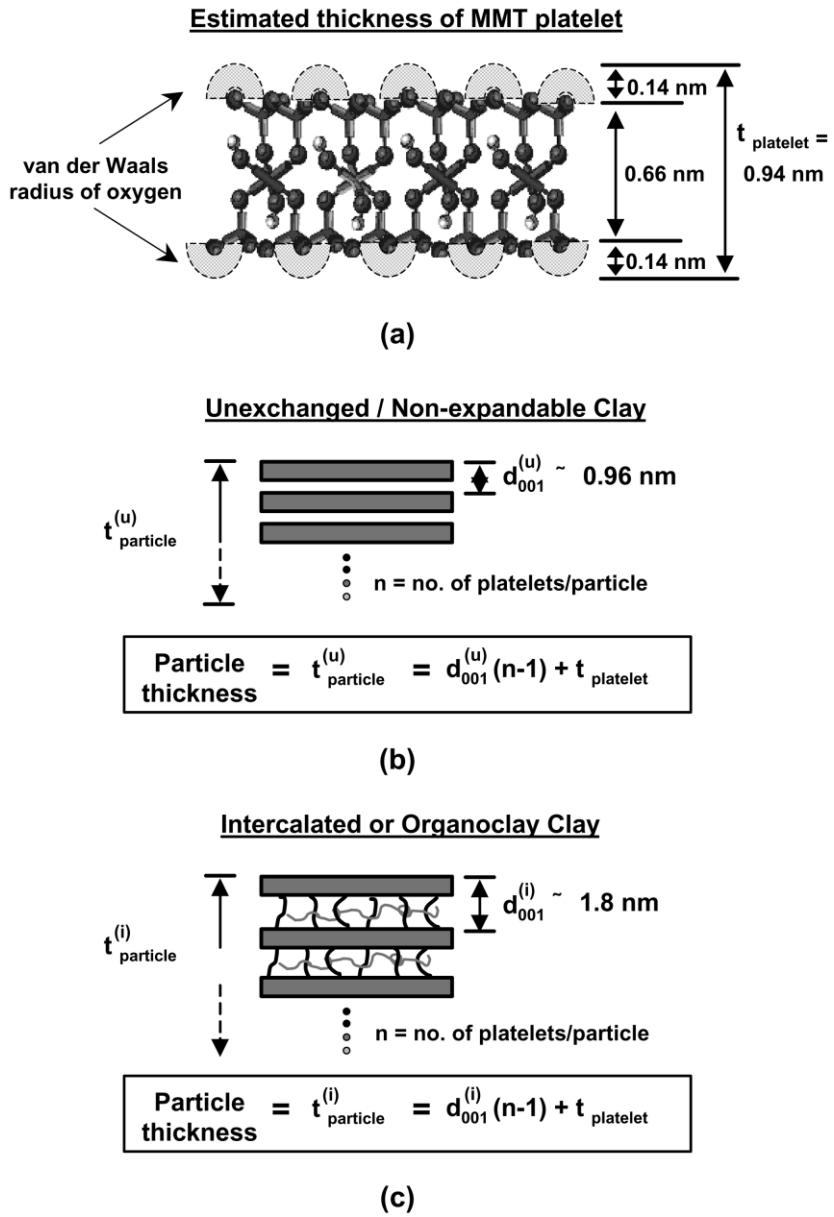

Fig. 9. Details of thickness calculation of (a) an individual MMT platelet, (b) an unexchanged or non-expandable clay stack, e.g. sodium MMT or talc-like clay, (c) an organoclay stack intercalated with surfactant and polymer.

where $d_{001}^{(i)}$ is the repeat spacing for the intercalated clay or organoclay; previous work from this laboratory showed that $(HE)_2M_1R_1$ nanocomposites based on a low molecular weight nylon 6 material exhibited a mixed morphology of delaminated and unexfoliated platelets [26,27]. Wide angle X-ray analysis of this material revealed a broad reflection at 5° of 2θ, corresponding to a repeat spacing of ~1.8 nm. It is assumed that the stacks of platelets for the present $(HE)_2M_1R_1$ nanocomposites based on HMW nylon 6 have a $d_{001}^{(i)} \cong 1.8$ nm. The number average thickness thus becomes

$$\bar{t}_{\text{particle}}^{(i)} = \frac{\sum(d_{001}^{(i)}(n-1) + t_{\text{platelet}})}{N_{\text{total}}} = \frac{\sum(1.8n - 0.86)}{N_{\text{total}}} \quad (10)$$

where N_{total} is the total number of particles. Substituting averages from Fig. 8(b) into Eq. (10) yields a number average particle thickness of 1.61 nm ($\bar{t}_n$) and a weight average thickness of 2.43 nm ($\bar{t}_w$). Thus, $\bar{\ell}_n/\bar{t}_n = 91/1.61 = 57$ and $\bar{\ell}_w/\bar{t}_w = 118/2.43 = 49$ or more extreme values if mixed averages are used. Available composite theories do not give any guidance of which aspect ratio to use when there is a distribution of lengths and thicknesses.

4. Results and discussion

This section explains how filler aspect ratio, modulus, and orientation influence the extent of reinforcement for

these nylon 6 nanocomposites based on glass fibers or LAS using the Halpin–Tsai and Mori–Tanaka theories. In addition, model predictions for each type of composite are benchmarked against experimental data. As will be shown, the two theories in some cases give different predictions. Some discussion will be devoted in explaining the differences; however, it is not the intent of this paper to fully evaluate the relative merits or deficiencies of the theories themselves. Attention will be focused primarily on unidirectional reinforced composites. First, though, it is important to briefly elaborate on the material properties that are used for the modeling calculations.

Table 3 lists pertinent physical property data for the components that make up each composite [33–37]. As stated above, the matrix and filler materials are assumed to be linear elastic and isotropic; the possible limitations of these assumptions for injection molded specimens are clearly evident. The values for the nylon 6 moduli were taken from the experimental data listed in Table 2; whereas, the filler moduli are experimental values reported in the literature. The modulus of MMT is assumed to be equal to that of muscovite [36,37], a mica-based layered silicate very similar in structure to MMT [33]. Early investigations by Alexandrov and Ryshova showed the modulus of muscovite could be determined using an ultrasonic pulse method [36]. They found that the stiffness within the basal plane, i.e. parallel to both the 1 and 2 directions as presented in Fig. 2(a), was isotropic and had a value of 178 GPa. Similar studies by McNeil and Grimsditch on muscovite using Brillouin scattering techniques gave identical results [37]; the shift in Brillouin frequency, ν, of an incident photon caused by a material is similar in theory to what happens to the speed of sound when an ultrasonic pulse is applied instead. Both events are related to the elastic modulus of the material in a given direction by the following equation

$$E = \rho\left(\frac{\nu}{q}\right)^2 = \rho v^2 \tag{11}$$

where ρ is the density, ν is the Brillouin frequency shift, q is the photon wave vector [37], and v is the sound velocity. The value of 2.83 g/cm^3 for the density of a MMT platelets reported in Table 3 was calculated from the unit cell weight of sodium montmorillonite, the surface area of 0.515×8.9 nm^2 [33], and a thickness of 0.94 nm indicated earlier in Fig. 9(a). This density agrees closely with the calculated values of phyrophllite and talc, 2.85 and 2.79 g/cm^3, respectively [34]. Last, the nylon 6 matrix is assumed to have a Poisson's ratio, ν_m, of 0.35, while the fillers are assumed to have a value of 0.20 [18,19].

4.1. Model calculations for nylon 6 composites based on glass fibers and LAS

Fig. 10 shows the effect of filler type and aspect ratio on the longitudinal reinforcement, $E_{\|}$, of nylon 6 as determined by the theories of Halpin–Tsai and Mori–Tanaka. Composites based on MMT in this case are treated as completely exfoliated. Special considerations such as stacks of immiscible or intercalated platelets are considered later. Fig. 10(a) shows that increasing the aspect ratio from 20 to 100 in both types of composites leads to a significant increase in reinforcement efficiency; however, this effect is more pronounced for the nanocomposites owing to the significantly higher modulus taken for MMT. The effect of filler modulus on reinforcement can be seen by comparing nanocomposite and glass fiber curves at the same aspect ratio. The nearly 2.5 fold difference in tensile modulus of MMT relative to glass fibers results in considerably steeper composite reinforcement curves. The combination of both high modulus and high aspect ratio leads to drastically different levels of reinforcement for the two materials. It is important to note that the Halpin–Tsai equations treat fibers and disks the same when the reinforcement is parallel to the test direction (see Fig. 2(a)).

The Mori–Tanaka theory, on the other hand, gives slightly different reinforcement trends for the two types of composites, as shown in Fig. 10(b). At an aspect ratio 20, the glass fiber composite is predicted to have a higher modulus than the corresponding MMT-based composite. This result can be explained by how the two theories treat filler geometry. As mentioned earlier, dispersed MMT platelets are expected to resemble disks. The Halpin–Tsai equations are identical in form when calculating longitudinal reinforcement for fibers and disks; whereas, the Mori–Tanaka theory treats the two geometries differently. For a given filler modulus and aspect ratio, the Mori–Tanaka predicts that unidirectional reinforcement by fibers is considerably greater than that

Table 3
Component physical property data used in composite modeling

Material	Young's modulus (GPa)	Density (g/cm^3)	Poisson's ratio	References
Glass-fiber composites				
MMW nylon 6	2.82	1.14	0.35	[18,19,35]
E-glass	72.4	2.54	0.20	[18,19,35]
LAS composites				
HMW nylon 6	2.75	1.14	0.35	[18,19,35]
MMT	178	2.83	0.20	[33,34,36,37]

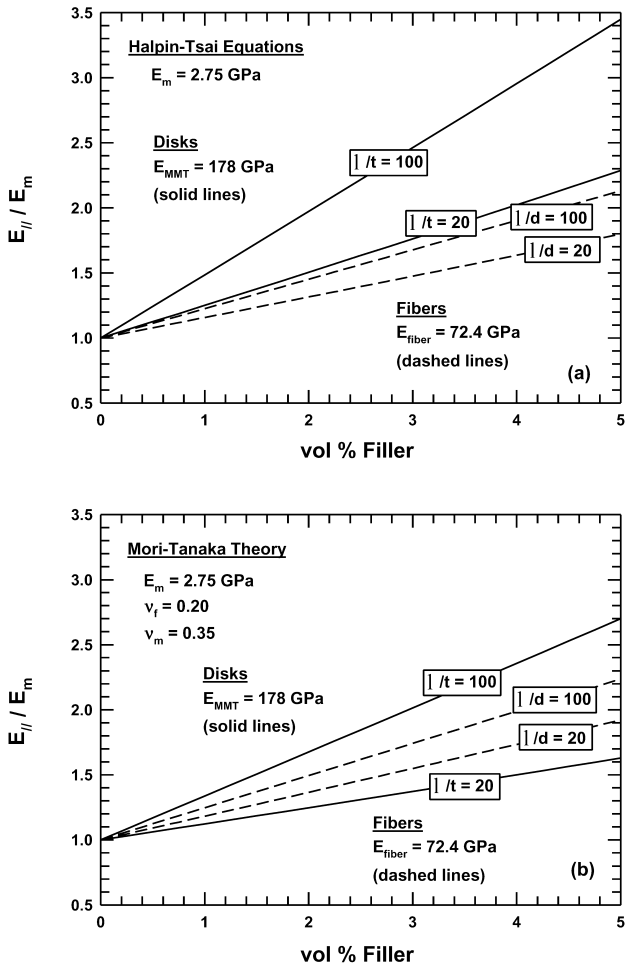

Fig. 10. Longitudinal reinforcement curves for nylon 6 composites based on MMT disk-like platelets and glass fibers predicted using the (a) Halpin–Tsai equations and (b) the Mori–Tanaka theory. Solid lines represent MMT disk reinforced composites; whereas, dashed lines represent glass fiber reinforced composites.

by disks. Unlike fibers, disks can be thought to have a range of aspect ratios if one thinks of subdividing the disk into fibers (of square cross-section) pointing in the direction of the applied force (Fig. 3). From the edges, the length of these imaginary fibers increases from zero to the platelet diameter at the center; thus the effective length of the disk will be less than its diameter. The ends or edges of the filler reduce the efficiency of load transfer by acting as weak points and sites of high stress concentration in the matrix. This effect becomes less pronounced with increasing aspect ratio, yet it persists to higher aspect ratios for disks than for fibers, this is again due to very low effective aspect ratios experienced at the extremities of the disk. From Fig. 10(b) it is seen that the Mori–Tanaka theory predicts that nanocomposite stiffness is more dependent on aspect ratio than is the case for glass fiber composites. Thus, at high aspect ratios, the level of reinforcement is predicted to be higher for the nanocomposite than for the glass fiber composite which reflects the higher modulus of MMT. In general, both theories emphasize the strong effects of filler modulus and aspect ratio.

A more comprehensive examination of how the two theories respond to filler geometry, aspect ratio, and modulus is given in Fig. 11. Fig. 11(a) shows the modulus predictions of the Halpin–Tsai equations which give the same $E_{\|}$ for disk and fiber reinforcement. As expected,

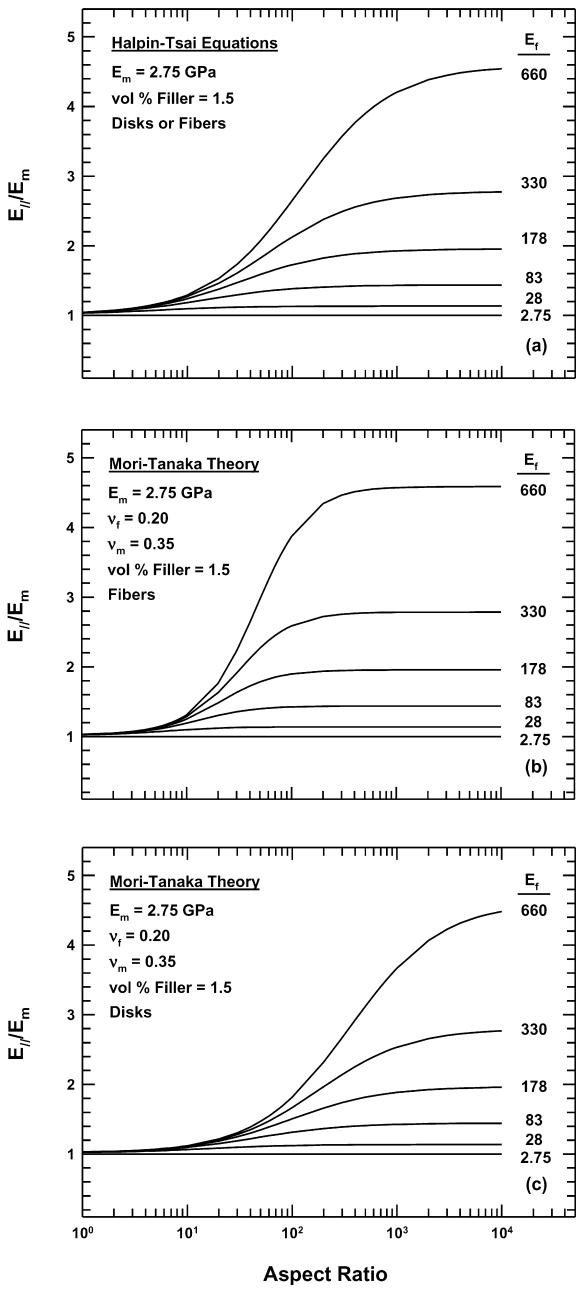

Fig. 11. The effect of filler aspect ratio and modulus on the longitudinal reinforcement of composites based on fiber and disk-like fillers as determined by (a) Halpin–Tsai equations (fibers or disks) and the Mori–Tanaka theory for (b) fiber and (c) disk reinforcement.

increasing the aspect ratio results in higher reinforcement for a given filler modulus and concentration. Likewise, increasing the filler modulus also improves the reinforcement especially for aspect ratios greater than 20–30; interestingly, recent molecular dynamics simulations by Rutledge [38] predict that the modulus of a single aluminosilicate sheet is significantly higher than the experimentally value of 178 for MMT reported here. If the modulus of MMT is indeed higher, it would have an even more pronounced effect on nanocomposite stiffness as demonstrated in Fig. 11(a). Analogous predictions from the Mori–Tanaka theory are given in Fig. 11(b) and (c) for fibers and for disks. The trends are qualitatively the same as in Fig. 11(a) but differ quantitatively. The Mori–Tanaka theory predicts fiber reinforcement to have a stronger dependence on aspect ratio at a given filler modulus than does the Halpin–Tsai, this theory predicts lower reinforcement at low aspect ratios from disks than does the Halpin–Tsai equations. Each theory, however, does asymptote to the same values for very high filler aspect ratios corresponding to the rule of mixtures, i.e. Eq. (4). Overall, the trends in Fig. 11 demonstrate considerable potential for improvement in nanocomposite stiffness by increasing the aspect ratio, whether from improvements in platelet exfoliation, synthesis of high aspect ratio clays, reduced platelet attrition, or other means.

In addition to aspect ratio and filler modulus, the orientation of the dispersed phase has a dramatic effect on modulus. From a practical standpoint, nearly all composites contain some degree of filler misalignment. Deviations from unidirectional reinforcement can result in sizable reductions in composite stiffness and this effect may be amplified depending on the shape of filler. It is apparent from their geometry, that disk-like platelets can provide equal reinforcement in two directions, if appropriately oriented, while fibers provide primary reinforcement in one direction. This difference becomes especially critical when the filler begins to deviate from unidirectional alignment. In the case of completely random orientation in all three orthogonal directions, platelets will inherently provide more effective reinforcement than fibers; this is shown quantitatively by the following equations

$$E_{\text{ran-3D}}^{\text{fibers}} = 0.184E_{\parallel} + 0.816E_{\perp} \tag{12}$$

$$E_{\text{ran-3D}}^{\text{platelets}} = 0.49E_{\parallel} + 0.51E_{\perp} \tag{13}$$

where $E_{\parallel}$ and $E_{\perp}$ are the composite moduli parallel (longitudinal) and perpendicular (transverse) to the major axis of the filler, respectively; these equations are approximations derived by van Es et al. using laminate theory [18,39]. Fig. 12(a) and (b) shows the effect of filler orientation on stiffness reinforcement, calculated by substituting results from the Halpin–Tsai equations and the Mori–Tanaka theory into Eqs. (12) and (13). For random 3D reinforcement, platelets lead to significantly higher stiffness enhancement in nylon 6 than do fibers having the same modulus, regardless of the theory used. Each curve for random orientation, however, still lies far below the corresponding curves for unidirectional orientation. Last, it should be pointed out that the random fiber reinforcement will be even lower when the filler has a modulus comparable to that of glass fibers.

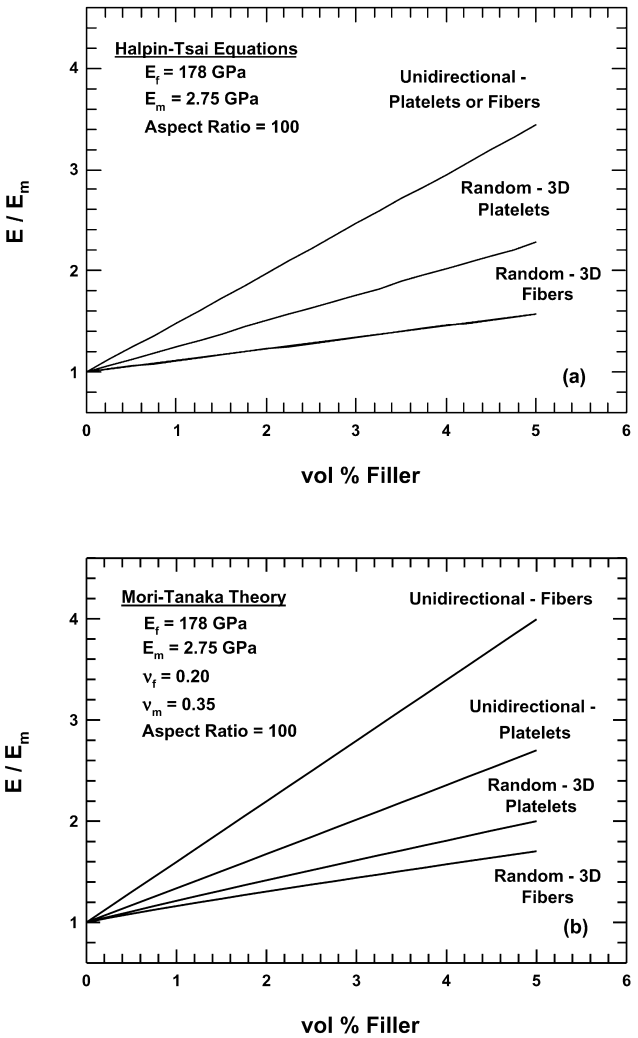

Fig. 12. The effect of fiber and platelet fillers on the reinforcement of nylon 6 as determined by (a) Halpin–Tsai equations and (b) the Mori–Tanaka theory.

The predictions in Figs. 10–12 demonstrate that the modulus, aspect ratio, shape, and orientation of the filler have dramatic effects on the final composite modulus. The results reflect how filler stiffness and fiber ends, or platelet edges influence load transfer from the matrix to filler. Rigid fillers are naturally resistant to straining due to their high moduli. When a relatively softer matrix is reinforced with such fillers, the polymer, particularly that adjacent to the filler particles, becomes highly restrained mechanically; this enables a significant portion of an applied load to be carried by the filler, assuming that the bonding between the two phases is adequate. Logically, the higher the filler modulus

is, the greater the restraint encountered by the matrix and, thus, the greater the stress transfer. Fiber ends or platelet edges, on the other hand, act as weak points and are sites of high stress concentration in the matrix. Increasing the aspect ratio of the filler, however, reduces this effect by increasing the amount of stress transferred to the filler. Last, orientation of the filler relative to the applied load will dictate the mechanism of stress transfer. When the filler is misaligned, or in the extreme case perpendicular to the applied load, the stress at the interface transforms from a shear mode into a tensile mode; this generates a higher concentration of stress in the matrix and less tension in the filler particle, which is similar to what happens at the end of a fiber or the edge of a platelet.

The shear lag theory developed by Cox [40] is useful to show how filler aspect ratio and modulus are related to stress transfer in a composite. The axial tension experienced in a dispersed short fiber exposed to an external strain was shown by Cox to be

$$\sigma_f = E_f \varepsilon_1 \left\{ 1 - \left[\frac{\cosh\left(na \frac{2x}{\ell} \right)}{\cosh(na)} \right] \right\} \tag{14}$$

where E_f is the Young's modulus of the filler, ε_1 is the applied strain, a is the fiber aspect ratio, ℓ/d, and x is the distance from the center of the fiber. The factor n is defined by

$$n = \sqrt{\frac{2G_m}{E_f \ln(2R/d)}} \tag{15}$$

where G_m represents the shear modulus of the matrix and $2R$ is the distance between the fiber and its nearest neighbor. It is important to note that this theory assumes the matrix and the filler are well bonded, which in reality may not be the case. A similar shear-lag theory by Shia et al. [20] treats the interfacial shear stresses experienced between a rectangular silicate platelet and a polymer matrix under imperfect bonding conditions.

Fig. 13(a) shows how fiber tensile stress, normalized to the applied strain, varies along short fibers of different aspect ratios; the shear modulus of the matrix in this plot is that of nylon 6 and was calculated assuming isotropic conditions using the polyamide's Young's modulus and Poisson's ratio (Table 3). Increasing the aspect ratio not only increases the amount stress the fiber is cable of carrying, it also minimizes the end effects, as seen by the sharper increase in σ_f along the extremes of the fiber. Increasing the filler modulus also increases σ_f as seen in Fig. 13(b); however, the curves are less abrupt at the fiber edges; this is a result of a larger mismatch between the shear modulus of the matrix and the Young's modulus of the filler. Larger ratios of G_m/E_f improve the stress transfer. Ultimately, it is the combination of high filler aspect ratio and modulus that enables fillers to bear a large portion of the applied load. Fig. 13(c) shows this synergistic effect on average fiber tension, $\bar{\sigma}_f$, defined by

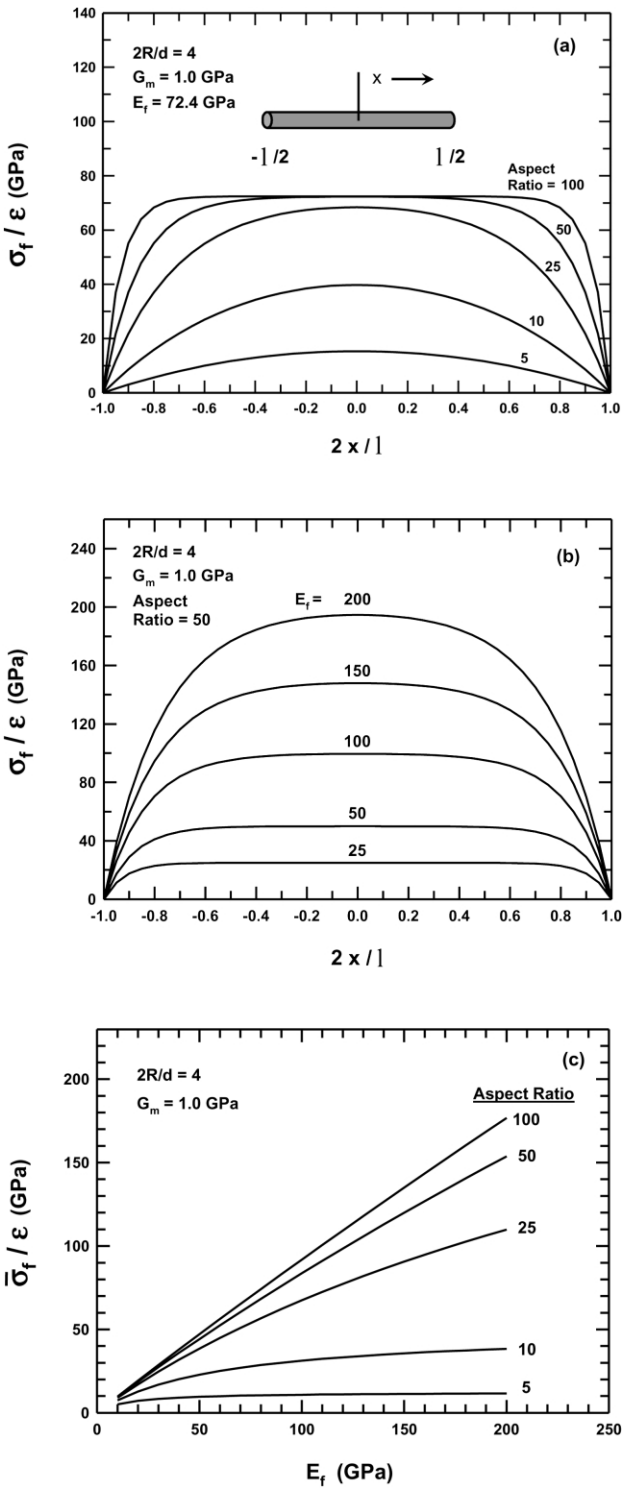

Fig. 13. Axial tension experienced along a fiber of length ℓ as a function of filler (a) aspect ratio and (b) modulus and (c) the combined effects of filler aspect ratio and modulus on the average fiber tension.

$$\bar{\sigma}_f = E_f \varepsilon_1 \left\{ 1 - \left[\frac{\tanh(na)}{na} \right] \right\} \tag{16}$$

Based on these simple considerations from composite theory, it becomes clear that the combination of high modulus and aspect ratio of MMT are the reasons for the better reinforcement in the nanocomposite than the glass fiber composite illustrated in Fig. 1.

4.2. Special considerations for polymer LAS nanocomposites

A key issue in forming polymer nanocomposites is achieving high levels of platelet exfoliation in a variety of polymer matrices. However, in most cases, exfoliation is thermodynamically unfavorable and most synthesis processes only lead to intercalated or immiscible systems. This section attempts to understand how incomplete exfoliation influences nanocomposite stiffness using composite theory.

For this analysis, the stacking of platelets within a particle is treated in a very simple fashion, i.e. platelets of equal diameter are stacked directly on top of one another and the applied load is parallel to the platelet edges, as shown in Fig. 14(a). In reality, however, stacking is not uniform, platelets vary in length, and notably the particles are not perfectly aligned in the direction of the applied load (Fig. 14(b)); thus, the forces on a stack become quite complex, and such factors as stack shear modulus and the strength of the interfacial bond between platelets and the polymer become increasingly important. Understanding of these types of stacking modes and how they affect nanocomposite modulus is at a primitive state and beyond the scope of this work; therefore, only the simplified case is examined here. The tensile modulus of a simple stack in the direction parallel to its platelets can be estimated by using the rule of mixtures, as previously suggested by Brune and Bicerano [23]

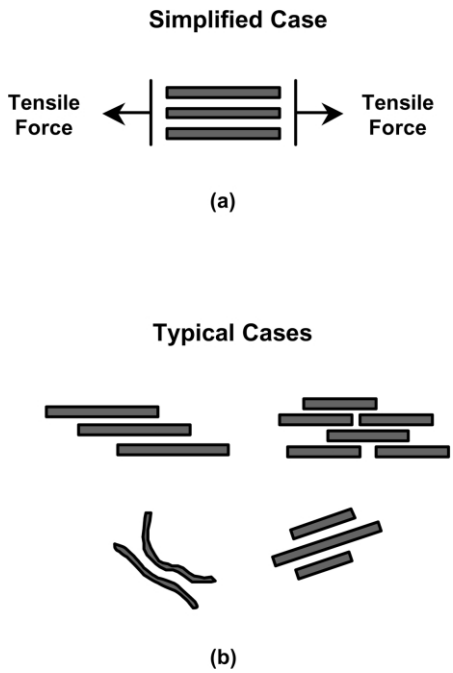

Fig. 14. Depiction of platelet organization for incompletely exfoliated particles: (a) simplified case and (b) typical cases.

$$E_{\text{stack}} = \phi_{\text{MMT}} E_{\text{MMT}} + \phi_{\text{gallery}} E_{\text{gallery}} \tag{17}$$

where ϕ_{MMT} is the volume fraction of silicate layers in the stack, E_{MMT} is the modulus of MMT, ϕ_{gallery} is the volume faction of gallery space, and E_{gallery} is the modulus of the material in the gallery which is expected to be much less than E_{MMT}. The volume fraction occupied by gallery space, ϕ_{gallery}, is simply the ratio of total gallery thickness over the thickness of the entire stack. This ratio can also be expressed in terms of X-ray d-spacings

$$\phi_{\text{gallery}} = \frac{(n-1)(d_{001} - t_{\text{platelet}})}{d_{001}(n-1) + t_{\text{platelet}}} \tag{18}$$

where n is the number of platelets per stack, d_{001} is the repeat spacing between silicate platelets, and t_{platelet} is the thickness of a silicate platelet, as defined in Fig. 9(a). Since a majority of the clay morphologies encountered in polymer nanocomposites can be lumped into two categories, unexchanged or non-expandable clay (Fig. 9(b)) and intercalated or organically modified clay (Fig. 9(c)), two different repeat spacings are evaluated, $d_{001} = 0.96$ nm ($d_{001}^{(u)}$) and $d_{001} = 1.8$ nm ($d_{001}^{(i)}$). Note, that when the number of platelets in a stack is equal to one, either system represents an individual exfoliated platelet having a modulus equal to 178 GPa.

Fig. 15(a) shows the effect of the number of platelets per stack on the modulus of these particles in the direction parallel to the platelets for the two types of clay basal spacings. For $d_{001} = 0.96$ nm, there is little change in modulus with increasing n; this is due to the very small volume contribution that gallery spacing provides to the overall stack volume. On the other hand, when the gallery volume is comparable to the volume occupied by the silicate platelets, i.e. $d_{001} = 1.8$ nm, the stack modulus drops abruptly with increasing n, eventually asymptoting to a value of 93 GPa; a d-spacing of 1.8 nm is a typical value for an organoclay or a stack mildly intercalated with polymer. Higher d-spacings can be seen and reflect high levels of polymer intercalation. This, of course, further decreases, to a certain degree, the stack modulus for a given value of n. In addition to modulus reduction, increasing the number of platelets per stack will inherently reduce the particle's aspect ratio. Fig. 15(b) shows the effect of n on stack aspect ratio. Both curves drop considerably with increasing n; however, the curve for the intercalated clay curve decreases at a faster rate, which is a direct result of a larger d-spacing.

To assess the effect of the two types of stacking on nylon 6 nanocomposite modulus, values obtained from Eq. (17) were substituted into the Halpin–Tsai and Mori–Tanaka equations. Since modulus is essentially a linear function of filler concentration at typical concentrations for nanocomposites, comparisons can be conveniently made in terms of the initial slope of the modulus versus concentration curve

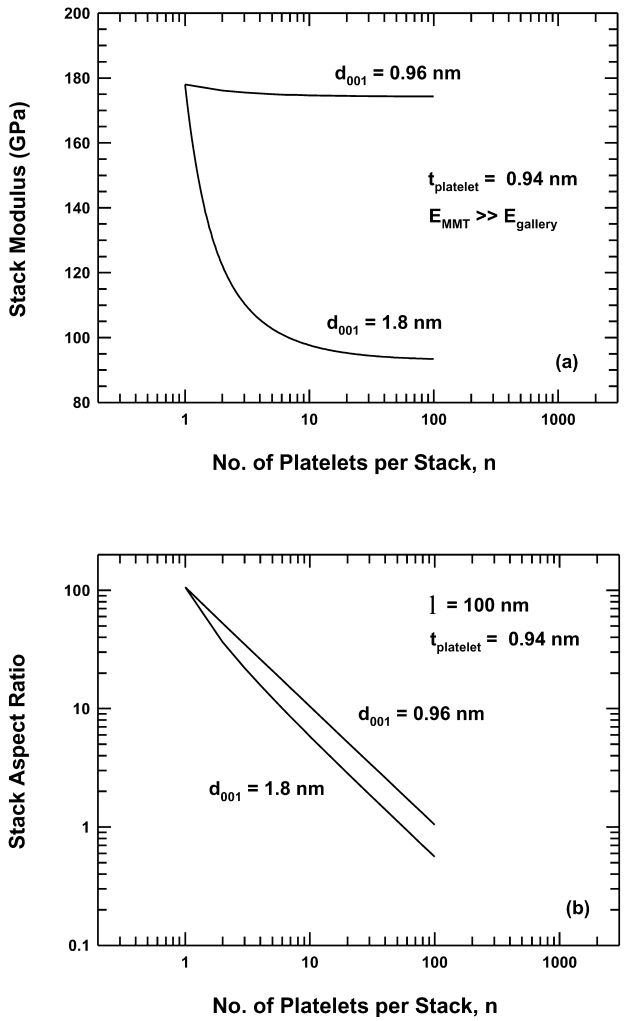

Fig. 15. The effect of the number of platelets per stack on the (a) modulus and (b) aspect ratio for the simplified arrangement of platelets as depicted in Fig. 14(a).

as defined by the following reinforcing factor

$$\text{Reinforcing Factor(RF)} = \lim_{\phi \to 0} \left\{ \frac{\mathrm{d}(E/E_{\mathrm{m}})}{\mathrm{d}\phi} \right\} \tag{19}$$

Table 4 shows how the number of platelets in a stack affects the reinforcement of nylon 6 by MMT in terms of this reinforcing factor, RF. Increasing n in both stacking scenarios leads to lower reinforcement efficiencies, especially for the intercalated clay case. Interestingly, the largest drop in reinforcement is experienced when going from one platelet to two platelets per stack. Overall, the trends in Table 4 show the high sensitivity of nanocomposite stiffness to the level of exfoliation. Stacks of platelets reduce nanocomposites stiffness through both the reduced aspect ratio and lower effective filler moduli. Furthermore, the trends agree with the more generalized approach taken by Brune and Bicerano [23] using the Halpin–Tsai equations, in which the moduli of the components and ratio of platelet thickness to gallery height were allowed to vary.

4.3. Benchmarking theory versus experiment: glass fiber composites

Fig. 16 shows experimental moduli of nylon 6 composites a as function of glass fiber content. The initial addition of glass fibers, i.e. up to 10 vol%, is less effective than at higher fiber contents. This lower reinforcing efficiency is believed to stem from low fiber orientation along the FD. Higher filler levels result in filler–filler interactions and this, plus the significantly increased melt viscosity, may subsequently alter the morphology of the injection molded composites, e.g. increased fiber orientation. Incomplete mixing may also be an issue here since the diluting matrix, MMW nylon 6, differs from that of the nylon 6 used in the BKV 30 master batch. SEM studies on these and similar composites revealed a mixed morphology in which the fibers in the outer portion (skin) of the specimen are highly aligned; whereas, those in the inner portion (core) are more randomly oriented [25]. Furthermore, composites containing higher concentration of fibers, i.e. those containing 16 vol%, exhibited a higher amount of orientation in the center of the bar than composites based on lower fiber concentrations, i.e. 2.3 vol% (5 wt%). Such morphological effects are consisted with the observation of others involving discontinuous fiber composites [41–43].

Fig. 16 also shows theoretical curves for two different morphologies, unidirectional fiber alignment and random three dimensional fiber orientation; the curves for random order were generated using Eqs. (12) and (13).

Table 4
Predicted reinforcing factors per number of platelets per stack

No. of platelets per stack	Reinforcing factor (RF) Halpin–Tsai equations[a] d_{001} = 0.96 nm	d_{001} = 1.8 nm	Mori–Tanaka theory[a] d_{001} = 0.96 nm	d_{001} = 1.8 nm
1	49.2	49.2	34.8	34.8
2	39.7	27.5	23.8	16.6
3	33.5	21.1	18.3	11.7
4	29.0	17.5	14.9	9.3
5	25.6	15.1	12.7	7.8
10	16.3	9.3	7.5	4.6

[a] Calculations were performed using a platelet length of 100 nm, a stack Poisson's ratio of 0.20, and matrix properties for HMW nylon 6.

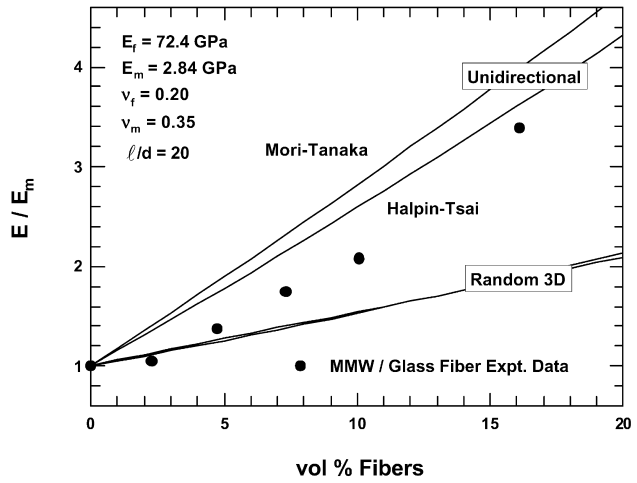

Fig. 16. Experimental modulus data for glass fiber reinforced nylon 6 and model predictions based on the experimentally determined aspect ratio of 20.

The Mori–Tanaka unidirectional curve is slightly higher than the Halpin–Tsai curve; whereas, both theories given nearly the same results for the random case. It should be emphasized that both theories are very sensitive to filler aspect ratio for unidirectional reinforcement, but relatively insensitive for random reinforcement; this means that the data are in closer agreement to the aligned case, which is consistent with the actual morphology. Both theories satisfactorily capture the response of stiffness to glass fiber content given the complex morphology.

4.4. Benchmarking theory versus experiment: LAS nanocomposites

Previous morphological studies on $(HE)_2M_1R_1$/HMW nylon 6 nanocomposites revealed high levels of platelet exfoliation [26,27]. In addition, further TEM analysis of sections taken from the central portion of injection molded specimen along the three principle directions showed that the platelets exhibit high degrees of orientation parallel to the FD [28]; photomicrographs from these studies are as shown in Figs. 7(a) and 17(a), while Fig. 5(a) above provides a pictorial description. This morphology is contrary to what is seen in the core portion of fiber reinforced composites, where a sizeable fraction of the filler is randomly oriented. Factors that contribute to the higher alignment of the LAS particles are their disk-like shape, high aspect ratio, and, collectively, large surface areas. Numerous applied and theoretical rheological studies have shown that plate-like particles align with their major axis in the FD [44–46]. For example, Schmidt et al. [46] showed using SAXS that under shear laponite platelets in PEO/water solutions become highly oriented along the direction of flow [46]. As expected, the morphology in the skin region of the present injection molded nanocomposites exhibits even higher degrees of platelet alignment than in the core, as seen in Fig. 17(b); this is, of course, due to the elevated

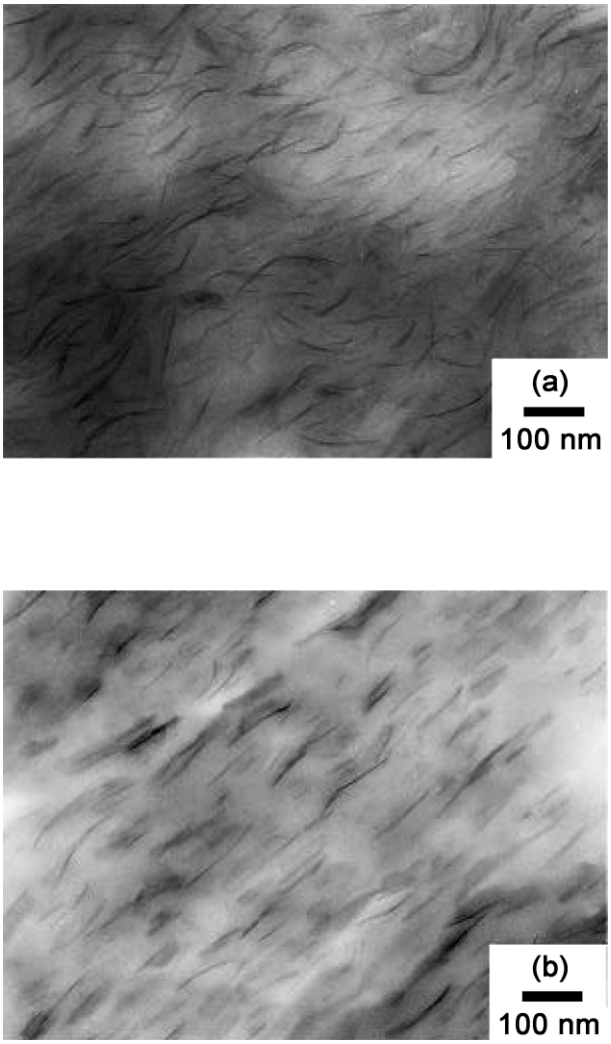

Fig. 17. TEM photomicrographs of HMW nylon 6-$(HE)_2M_1R_1$ nanocomposites (~ 3 wt% MMT) taken of the (a) core and (b) skin parallel to the FD axis. TEM sections were extracted from the TD–ND plane.

levels of stress experienced at the mold surface during injection molding. Given this observed morphology, benchmarking of composite theory against experimental data can be done confidently assuming unidirectional alignment.

Fig. 18(a) compares experimental modulus data for the $(HE)_2M_1R_1$/HMW nylon 6 nanocomposites with model predictions for aligned LAS nanocomposites having an aspect ratio identical to the experimental value of 57 (number average aspect ratio), and a ratio of 97, corresponding to perfectly exfoliated morphology, i.e. the number average particle length, 91 nm, divided by the thickness of an individual platelet, 0.94 nm. The Halpin–Tsai equations for $\ell/t = 57$ slightly overpredicts the experimental data, while the Mori–Tanaka theory underpredicts the experimental data. Overall, the theories of Halpin–Tsai and Mori–Tanaka capture the observed nanocomposite stiffness behavior. Both theories demonstrate that even higher levels of reinforcement could be

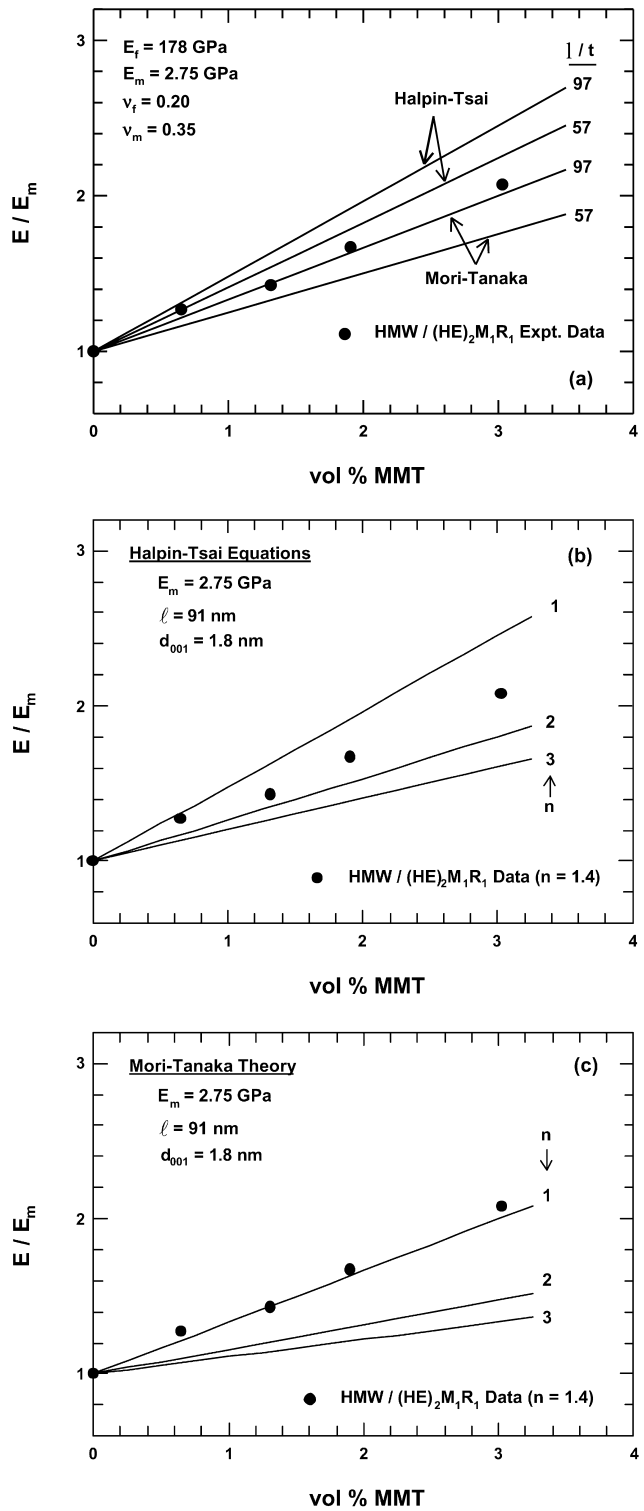

Fig. 18. Experimental and theoretical stiffness data for HMW nylon 6 nanocomposites; model predictions are based on unidirectional reinforcement of (a) pure MMT having a filler modulus of 178 GPa and aspect ratio of 57 (experimentally determined number average value) and 97, corresponding to complete exfoliation, and (b,c) stacks of clay intercalated with polymer having one or more platelets per stack. Note that experimental modulus data is plotted versus vol% MMT, since MMT is the reinforcing agent.

achieved by higher levels of exfoliation, larger platelet diameters, improved orientation, etc.

It is also useful to compare experimental data to model predictions based on an unexfoliated morphology, since the actual morphology contains a significant fraction of stacks of platelets. Fig. 18(b) and (c) compares the experimental moduli to theoretical curves calculated from the theories of Halpin–Tsai and Mori–Tanaka using Eqs. (17) and (18). Stack properties are based on experimental data, i.e. the stacks are 91 nm in length, have a repeat spacing of 1.8 nm, and each individual disk has a modulus of 178 GPa; experimental moduli are plotted versus vol% MMT since it is the reinforcing component. The experimental data fall between the Halpin–Tsai curves corresponding to 1 and 2 platelets per stack, as seen in Fig. 18(b), which is very close to the experimental determined value of 1.4. The experimental data matches a completely exfoliated morphology, i.e. $n = 1$, when the Mori–Tanaka theory is used.

4.5. Dynamic mechanical properties of LAS nanocomposites

4.5.1. DMTA experimental results and discussion

Fig. 19 shows the effect of temperature and filler concentration on the dynamic mechanical properties of nylon 6 nanocomposites. Dispersing MMT within the polyamide results in a considerable increase in stiffness at all temperatures, as shown by the plot of storage modulus (Fig. 19(a)). The reinforcing effect is greatest in the region above the glass transition temperature, T_g, of the matrix; this is primarily due to the larger difference in mechanical properties between the filler and the matrix as it goes from the glassy to the rubbery state. The filler, on the other hand, remains rigid throughout the entire temperature range. Interestingly, at temperatures between T_g and T_m the nanocomposites exhibit a greater decrease in modulus than does the pure polyamide; several possible reasons may be responsible. For example, the type of crystalline form of nylon 6 may affect the response of stiffness to temperature. Previous studies have shown that nanocomposites often have a higher fraction of the γ crystalline form of nylon 6; whereas, pure nylon 6 generally exhibits more of the α-form [1,47–49]. Interestingly, Ito et al. [50] showed that the two forms have different mechanical properties, specifically higher draw ratios of nylon 6 fibers were achieved between 110 and 180 °C when the γ-crystalline form is present as compared to the α-form The size of the polymer crystallites may also influence stiffness properties. Studies have shown that the polymer crystallite size is considerably smaller in nanocomposites than in the pure polyamide [51].

Fig. 19(b) shows the effect of clay concentration on T_g, represented by the tan δ peak location. Although there is little difference in T_g between the materials, there is a slight increase in T_g with increasing MMT concentrations at levels between 1.6 and 7.2 wt% MMT; this may be due to polymer-filler interactions. It is worth noting that the height of the tan δ peaks

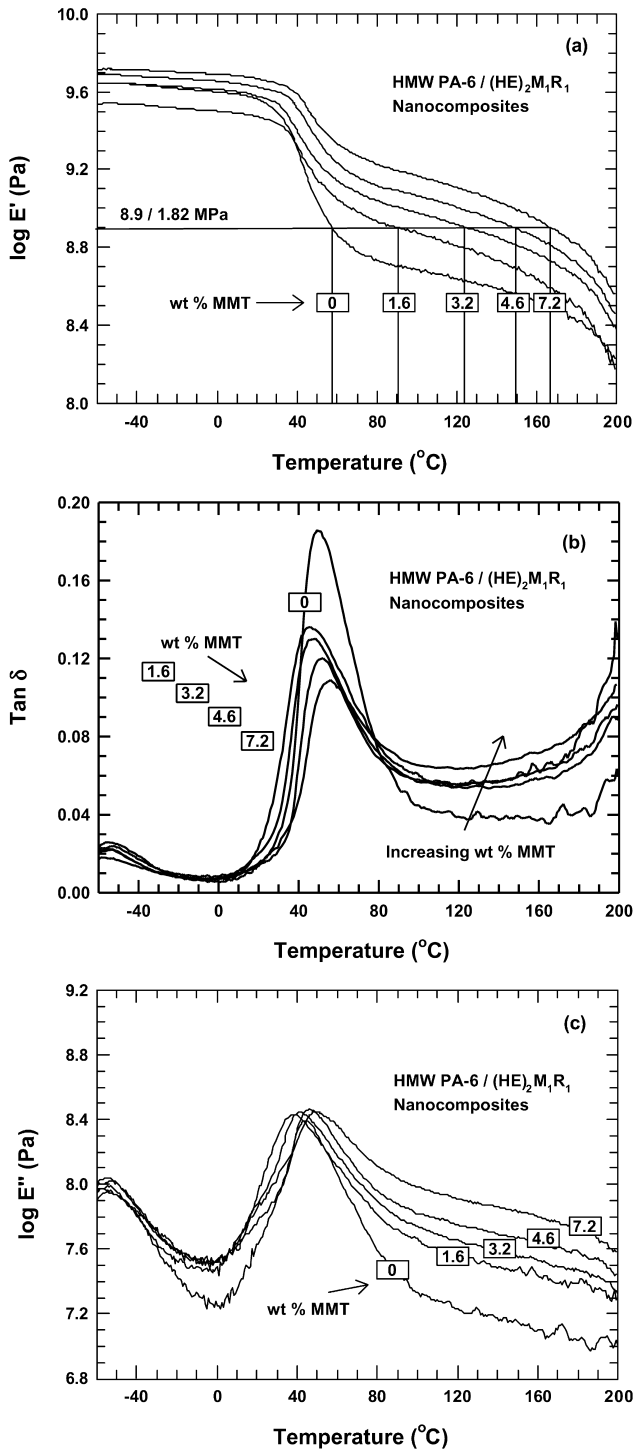

Fig. 19. Experimental dynamic mechanical data for HMW nylon 6-$(HE)_2M_1R_1$ nanocomposites: (a) storage modulus, E', (b) tan δ, and (c) loss modulus, E''. The technique used for estimating HDT is illustrated in the plot of log E' versus temperature.

decreases with increasing temperature. Some reports suggest this represents a suppression of the glass transition by the presence of the clay [52]. This conclusion, however, is a misinterpretation, since the low values for the nanocomposites are simply a result of dividing the relatively constant loss modulus, E'', values in the T_g region (Fig. 19(c)), by larger and larger storage modulus values, E'. Indeed, there is minimal difference between the E'' peak heights of the nanocomposites and the pure polyamide. Addition of clays does, however, increase the dampening effect at temperatures between T_g and T_m, as seen by the larger values of E'' in this region. This trend is common in reinforced polymers, particularly those reinforced with flake-like fillers [52,53].

As mentioned earlier, DMTA data can be used to estimate the HDT of a polymer [31]. Fig. 19(a) illustrates how the HDT defined at a stress of 1.8 MPa is estimated using DMTA storage modulus data. The temperature values obtained in Fig. 20 as function filler content; notably, the values reported here are very similar to those reported in the literature for melt processed [54] and in situ nylon 6 nanocomposites [55]. Adding small amounts of filler increases the HDT well above that of pure nylon, which occurs near the polyamide's T_g. However, beyond 2 vol% the rate of increase in HDT begins to diminish; this is to be expected since the HDT is approaching the melting point of the polymer. The large increase in HTD is the result of the shape of the modulus versus temperature curve and the increase in modulus by addition of the filler. Since nylon 6 is semi-crystalline polymer, some level of stiffness is maintained beyond T_g and up to T_m; this is evident by the shape of the log E' versus temperature curve in Fig. 19(a). It has been repeatedly shown that fillers typically increase the HDT of semi-crystalline polymers much more than for glassy polymers [53]. Thus, the high reinforcing efficiency of dispersed clay coupled is the principle cause of the large increase in HDT.

4.5.2. Theoretical prediction of heat distortion temperature

The increase in HDT due to filler can be calculated, in principle, by using composite theory to model the DMTA properties coupled with the method of Scobbo [31]. In what follows the Halpin–Tsai equations are used to predict storage modulus data as function of temperature for the

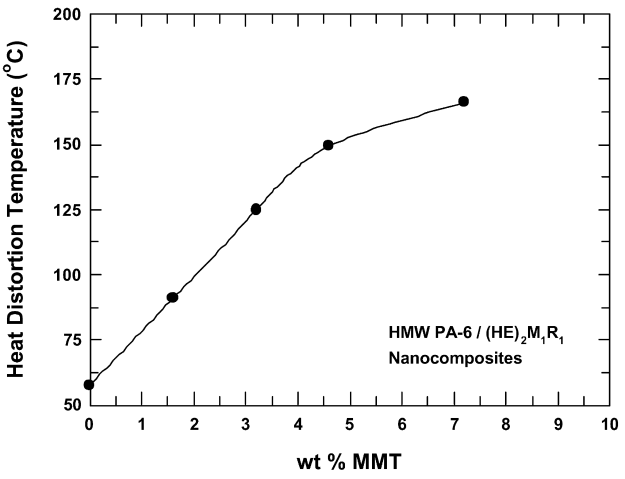

Fig. 20. Effect of MMT content on the HDT extracted from Fig. 19(a).

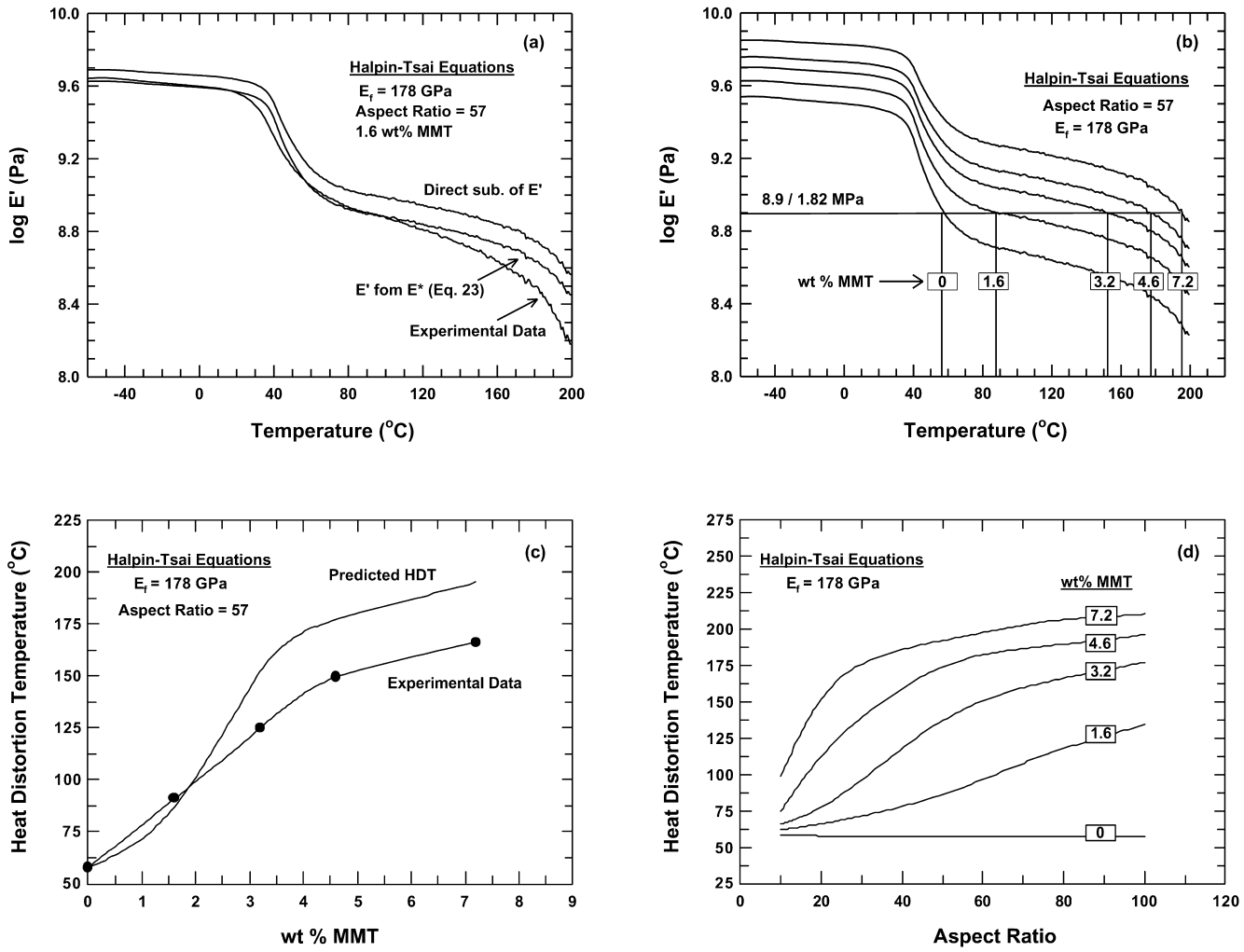

Fig. 21. Halpin–Tsai predictions for (a) log E' versus temperature using Eq. (23) and by direct substitution of E_m' for E_m in Eq. (1), (b) log E' versus temperature for all experimental MMT concentrations, (c) HDT versus MMT concentration (experimental data included) and (d) HDT versus aspect ratio at varying MMT concentration.

present nanocomposites. The complexity of the Mori–Tanaka theory makes prediction of DMTA data considerably more complex and, thus, was not performed here.

To model the DMTA data for composites, the complex moduli of the matrix

$$E_m^* = E_m' + iE_m'' \tag{20}$$

and the filler

$$E_f^* = E_f' + iE_f'' \tag{21}$$

must be substituted in the Halpin–Tsai equations in place of E_m and E_f, respectively. Since the stiffness properties of MMT are expected to be completely elastic and constant over the temperature range tested, the imaginary component is neglected, i.e.

$$E_f^* = E_f' + iE_f'' = E_f' = E_f \tag{22}$$

Combining Eqs. (1), (2), (20) and (22) and solving for the real component of the nanocomposite complex storage modulus yields

$$E' = \frac{1}{f}[ag(E_m'2 - E_m''2) - 2ahE_m'E_m'' + bgE_m' - bhE_m''] \tag{23}$$

where a, b, f, g, and h are functions of filler aspect ratio, volume fraction, E_m', and/or E_m''; details of these functions, as well as the expression for E', are given elsewhere [56]. To obtain an entire DMTA storage modulus versus temperature curve, storage and loss modulus values obtained from the DMTA analysis of pure HMW are substituted into Eq. (23) at each temperature tested.

Fig. 21(a) compares experimental storage modulus data with theoretical predictions assuming prefect exfoliation and unidirectional alignment of the filler in the direction of the applied load. Also included in this figure is the nanocomposite storage modulus obtained by direct substitution of E_m' for E_m in Eqs. (1) and (2) at each temperature. The $E'(T)$ curve obtained from Eq. (23) does an adequate

job at describing the experimental data over a broad range of temperatures; however, it begins to deviate from the data at about 110 °C and beyond. This disparity at high temperatures reflects the difference in the shape between the pure polyamide and the nanocomposite. In contrast to the predictions made using Eq. (23), the curve obtained by direct substitution fails to predict the experimental data over the entire range of the curve; previous modeling studies in the literature have largely overpredicted experimental data when using this direct substitution approach [18].

Fig. 21(b) shows $E'(T)$ curves predicted from Eq. (23) which may be compared to the experimental plots in Fig. 19(a). Fig. 21(c) compares experimentally determined HDT with those predicted using the Halpin–Tsai equations. In general, the model does a reasonable job at capturing the shape of the composite curve. The Halpin–Tsai theory should overpredict the data, since it assumes unidirectional alignment of the filler, whereas experimentally, this not the case. A large component of the overestimation, however, arises from the disparity of the $E'(T)$ curves for nanocomposite versus the pure polyamide at high temperatures. The overestimation increases with filler concentration and is very sensitive to small changes in log E'. Physical reasons may stem from crystalline morphology differences, filler concentration effects, i.e. agglomeration, decreases in particle aspect ratio, particle–particle interactions, etc. Last, Fig. 21(d) shows that increasing the aspect ratio beyond current levels would further improve the HDT, particular at low clay loadings.

5. Conclusions

The composite theories of Halpin–Tsai and Mori–Tanaka were employed to better understand the superior reinforcement observed for well-exfoliated nanocomposites relative to conventional glass fibers composites. The two theories differ in regard to their treatment of filler geometry; however, they both show analogous responses to how composite modulus responds to filler aspect ratio, modulus, and orientation. Theoretical comparisons for nylon 6 reinforced with montmorillonite (nanocomposites) versus glass fibers (conventional composites) show that the nanocomposites out-perform the glass fiber composites because of the high modulus and high aspect ratio of montmorillonite and its ability to reinforce in two directions. The theories were also used to examine the effect of incomplete exfoliation of simple stacks of montmorillonite, representing either sodium montmorillonite or clay intercalated with polymer. Increasing the number of clay platelets per stack causes a dramatic decrease in reinforcing efficiency which is a result of a reduction in both the aspect ratio and effective modulus of the clay stacks. Interestingly, the largest decrease in reinforcing efficiency is observed when going from one to two platelets per stack.

The two theories were benchmarked against experimental data for nylon 6 composites based on montmorillonite and glass fibers. Experimental determination of the clay characteristics, e.g. modulus, density, and in particular, aspect ratio, is not trivial. The lack of complete exfoliation of clay platelets, large variation of platelet lengths and particle thicknesses leads to many complex shapes and sizes, and ultimately a distribution of aspect ratios. Within these constraints, however, the two composite theories satisfactorily capture the experimental modulus behavior of the nylon 6 composites. Likewise, composite theory adequately describes the experimental HDT data obtained from DMTA properties of the nanocomposites. It is clear from the good agreement between the experimental data and the predictions of these models that the superior reinforcement and improved HDT for nylon 6 nanocomposites arises primarily from the combination of high modulus and aspect ratio of MMT, rather than from changes in the polymer matrix caused by the clay platelets.

Acknowledgements

This work was funded by the Air Force Office of Scientific Research. The authors would like to thank Professor Charles Tucker, III of the University of Illinois at Urbana-Champaign for his helpful comments regarding composite theory, Professor Necip Güven of Texas Tech University and Dr Simon Tsipursky for their input on MMT platelet thickness calculations, and Professor G.C. Rutledge of the Massachusetts Institute of Technology for showing the results of Ref. [38] prior to publication.

References

[1] VanderHart DL, Asano A, Gilman JW. Chem Mater 2001;13(10):3796–809.
[2] Anastasiadis SH, Karatasos K, Vlachos G, Manias E, Giannelis EP. Phys Rev Lett 2000;84(5):915–8.
[3] Zax DB, Yang DK, Santos RA, Hegemann H, Giannelis EP, Manias E. J Chem Phys 2000;112(6):2945–51.
[4] Halpin JC. J Compos Mater 1969;3:732–4.
[5] Halpin JC, Kardos JL. Polym Engng Sci 1976;16(5):344–52.
[6] Ashton JE, Halpin JC, Petit PH. Primer on composite materials: analysis. Stamford, Conn: Techomic Pub. Co; 1969.
[7] Hermans J. Proc Kon Ned Akad v Wetensch B 1967;65:1–9.
[8] Hill R. J Mech Phys Solids 1964;12:119.
[9] Foye R. SAMPE 1966;10:G-31.
[10] Adams D, Doner D. J Compos Mater 1967;1(4):152.
[11] Mori T, Tanaka K. Acta Metall 1973;21:571–4.
[12] Eshelby JD. Proc Roy Soc Long 1957;A241:376.
[13] Tandon GP, Weng GJ. Polym Compos 1984;5(4):327–33.
[14] Ramsteiner F. Composites 1981;12(1):65–71.
[15] Hsueh C-H. Compos Sci Technol 2000;60(14):2671–80.
[16] Biolzi L, Castellani L, Pitacco I. J Mater Sci 1994;29(9):2507–12.
[17] Chao L-P, Huang Y-S. Polym Compos 2000;21(1):20–7.
[18] van Es M, Xiqiao F, van Turnhout J, van der Giessen E. Comparing polymer–clay nanocomposites with conventional composites using composite modeling. In: Al-Malaika S, Golovoy AW, editors.

Specialty polymer additives: principles and applications. CA Malden, MA: Blackwell Science; 2001. Chapter 21.
[19] Hui CY, Shia D. Polym Engng Sci 1998;38(5):774–82.
[20] Shia D, Hui CY, Burnside SD, Giannelis EP. Polym Compos 1998; 19(5):608–17.
[21] Chow TS. J Mater Sci 1980;15(8):1873–88.
[22] Tucker III CL, Liang E. Compos Sci Technol 1999;59:655–71.
[23] Brune DA, Bicerano JU. Polymer 2002;43(2):369–87.
[24] Sheng N. Micro/nanoscale modeling of anisotropic mechanical properties of polymer/layered-silicate nanocomposites. Master's Thesis. Department of Mech Engng, Massachusetts Institute of Technology; 2002.
[25] Laura DM, Keskkula H, Barlow JW, Paul DR. Polymer 2000;41(19): 7165–74.
[26] Fornes TD, Yoon PJ, Keskkula H, Paul DR. Polymer 2001;42(25): 09929–40.
[27] Fornes TD, Yoon PJ, Keskkula H, Paul DR. Polymer 2002;43(7): 2121–2.
[28] Yoon PJ, Fornes TD, Paul DR. Polymer 2002;43(25):6727–41.
[29] Oshinski AJ, Keskkula H, Paul DR. Polymer 1996;37(22):4891–907.
[30] Fornes TD, Yoon PJ, Hunter DL, Keskkula H, Paul DR. Polymer 2002;43(22):5915–33.
[31] Paul DR, Bucknall CB. Polymer blends. New York: Wiley; 2000.
[32] Tsipursky SI, Drits VA. Clay Miner 1984;19:177–93.
[33] Van Olphen H. An introduction to clay colloid chemistry: for clay technologists, geologists, and soil scientists, 2nd ed. New York: Wiley; 1977.
[34] Clark SP, editor. Handbook of physical constants. New York: Geological Society of America; 1966. p. 50–89. rev. ed.
[35] Kohen MI. Nylon plastics handbook. New York: Hanser; 1995.
[36] Alexandrov KS, Ryshova TV. Bull Acad Sci, USSR, Geophys Ser 1961;12:1165–8.
[37] McNeil LE, Grimsditch M. J Phys: Condens Matter 1993;5(11): 1681–90.
[38] Manewitch OL, Rutledge GC. Submitted for publication.
[39] Hull D, Clyne TW. An introduction to composite materials, 2nd ed. New York: Cambridge University Press; 1996.
[40] Cox HL. Brit J Appl Phys 1952;3:72–9.
[41] Friedrich K. Plast Rubber Process Appl 1983;3(3):255–65.
[42] Karger-Kocsis J, Friedrich K. Compos Sci Technol 1988;32(4): 293–325.
[43] Karger-Kocsis J. Composites (Guildford, UK) 1990;21(3):243–54.
[44] Clarke SM, Rennie A, Covert P. Europhys Lett 1996;35:233–8.
[45] Yamamoto S, Matsuoka T. J Chem Phys 1997;107:3300–8.
[46] Schmidt G, Nakatani AI, Butler PD, Han CC. Macromolecules 2002; 35:4725–32.
[47] Lincoln DM, Vaia RA, Wang ZG, Hsiao BS, Krishnamoorti R. Polymer 2001;42(25):9975–85.
[48] Wu Q, Liu X, Berglund LA. Polymer 2002;43(8):2445–9.
[49] Fornes TD, Paul DR. Polymer 2003;44(14):3945–61.
[50] Ito M, Mizuochi K, Kanamoto T. Polymer 1998;39(19):4593–8.
[51] Ma J, Zhang S, Qi Z, Li G, Hu Y. J Appl Polym Sci 2002;83(9): 1978–85.
[52] Jimenez G, Ogata N, Kawai H, Ogihara T. J Appl Polym Sci 1997; 64(11):2211–20.
[53] Nielsen LE, Landel RF. Mechanical properties of polymers and composites. New York: Marcel Dekker; 1994. 2nd rev. and expand ed.
[54] Akkapeddi MK. Annu Technol Conf—Soc Plast Engineers 1999;57: 1619–22.
[55] Kojima Y, Usuki A, Kawasumi M, Okada A, Kurauchi T, Kamigaito O. J Polym Sci, Part A: Polym Chem 1993;31(4):983–6.
[56] Fornes TD. Polyamide-layered silicate nanocomposites by melt processing. PhD Dissertation, University of Texas at Austin, Chem Engng; 2003.